Synthesis and Optical properties of New Perylene Derivatives

Emile Muah Galabe

Submitted to the
Institute of Graduate Studies and Research
in partial fulfillment of the requirements for the Degree of

Master of Science
in
Chemistry

Eastern Mediterranean University
June 2014
Gazimağusa, North Cyprus

Approval of the Institute of Graduate Studies and Research

Prof. Dr. Elvan Yilmaz
Director

I certify that this thesis satisfies the requirements as a thesis for the degree of Master of Science in Chemistry.

Prof. Dr. Mustafa Halilsoy
Chair, Department of Chemistry

We certify that we have read this thesis and that in our opinion it is fully adequate in scope and quality as a thesis for the degree of Master of Science in Chemistry.

Prof. Dr. Huriye Icil
Supervisor

Examining Commmittee

1. Prof. Dr. Huriye Icil
2. Asst. Prof. Nur P. Aydinlik
3. Asst. Prof. Dr. Mustafa E. Ozser

ABSTRACT

Versatile substituents of perylene chrmophores creates higher absorptions in visible region of absorption spectrum and also exhibits higher coefficients of molar extinction. Furthermore, they have the ability to emit light of almost unitary which signifies higher fluorescence quantum yields. Perylene dyes acts a major role in dye sensitized solar cells due to the presence of four carbonyl groups in its core which creates ease of accepting an electron.

In this research, N,N′-Bis(3,3,5,5-tetramethyl-4-piperidinyl)-3,4,9,10-perylenebis (dicarboximide) (PPDI) and N-(3,3,5,5-tetramethyl-4-piperidinyl)-3,4,9,10-perylenetetracarboxylic-3,4-anhydride-9,10-imide (PPMI) were sensitized and comparison of their photophysical properties were carried out. FTIR spectroscopy was used to characterize the compounds and their photophysical properties analyzed via absorption and emission spectroscopy.

All the perylene dyes synthesized showed very high molar absorptivity with the highest being 152000 $M^{-1}cm^{-1}$ obtained from PPMI. PPMI absorption spectrum shows a 4 nm blue shift in a polar aprotic solvent as a result of increased level of polarity and the stabilization of PPMI energy levels it induces on the structure.

Keywords: Perylene diimide, perylene tetracarboxylic acid, perylene monoimde, perylene carboxylic acid monoimide.

ÖZ

Çok Yönlü atomuna no oluşturur perylene chrmophores emilimler daha yüksek görünen bölge absorpsiyon spektrumu ve olduysa da daha yüksek varyasyon katsayıları molar sönme. Ayrıca, ışık yaydığından yeteneğine sahip olan hemen hemen devletin üniter anlamına gelmektedir uygulandığında flüoresans üreten kendinden aydınlatmalı kuvantum verimleri daha yüksek. Görevi görür Perylene boyalar önemli bir rol boya pozlandırmadan güneş enerjisi hücreleri bulunması nedeniyle dört carbonyl grubu oluşturan, temel kabul kolaylığı bir elektron.

Bu araştırma, N, N' -Bis(3,3,5,5-tetramethyl-4-piperidinyl)-3,4,9,10-perylenebis (dicarboximide) (PPDI) ve N- (3,3,5,5-tetramethyl-4-piperidinyl)-3,4,9,10-perylenetetracarboxylic-3,4-anhidrit-9,10-imide (PPMI) pozlandırmadan ve karşılaştırma, photophysical özellikleri gerçekleştirildi. FTIR spektroskopi, karakterize etmek için kullanılan bileşikler ve onların photophysical özellikleri üzerinden analiz emilim ve emisyon spektroskopi.

Gösterdi Tüm perylene boyalar sentezlenmiş çok yüksek molar absorptivity olan en yüksek 152000 $M^{-1}cm^{-1}$ elde PPMI. PPMI absorpsiyon spektrumu 4 nm mavi gösterir vardiya kutup ayısı aprotic solvent sonuç olarak artan düzeyde polarite ve stabilizasyonu PPMI enerji seviyelerine yankılanmaya neden olur.

Anahtar Sözcükler: Perylene diimide, perylene tetracarboxylic asit, perylene monoimde, perylene carboxylic asit monoimide.

To my Father and Mother:

His Royal Majesty M.S.T Galabe II

Her Grace, Queen Cecilia Galabe

To my Sponsors:

Dr. Michael Nkemitag

Mrs. Stella Luma Nkemitag

ACKNOWLEDGEMENT

My sincere gratitude to Prof. Dr. Huriye Icil (my supervisor), for accepting me under her research team and Organic family, initiation of this study, stimulation, valuable criticism and support and for always guiding me with respect to research work under the faculty of Arts and Sciences.

My sincere thanks to Dr. Duygu Uzun for her willingness to technically drill me in the laboratory during the entire period of the research work and seeing into it that everything is concluded safely.

I also like to thank Dr. Babu J., Dr. Laure, the Organic family, Joy Foy, and Agustina Fru for all their helpful and constructive suggestions, critical comments and assistance during this study.

My gratitude to: the entire Royal House of Nepgahyidbi (Bali-Gham) especially my brothers and sisters for all their constant supports and encouragements throughout this study.

All the students present with me in the Laboratory and more especially the Organic Family.

My special thanks to Tetuh A. Lynda and Galabe Michael Z. for their patience and encouragements.

All my friends, Ayo I, Stella L, Zahra M, Marjan K, Rodrique N, Clovis M, Claude A, Evelyne B, Vivianne M, Cynthia N, Helen N, etc for their constant support and encouragement.

All my Nices and Nephews for all their constant prayers and calls of encouragement.

TABLE OF CONTENTS

LIST OF TABLES

LIST OF FIGURES

LIST OF ILLUSTRATIONS

LIST OF SYMBOLS

Å	Amstrong
cm	Centimeter
°C	Degrees Celcius
$\Delta\bar{\nu}_{½}$	Half-width of the selected Absorption
ε_{max}	Maximum Extinction Coefficient
E_s	Singlet Energy
f	Oscillator Strength
λ_{exc}	Excitation Wavelength
λ_{max}	Maximum Absorption Wavelength
τ_0	Theoretical Radiative Lifetime
τ_f	Fluorescence Lifetime
Φ_f	Fluorescence Quantum Yield
nm	Nanometer
$CHCl_3$	Chloroform
CHL	Chloroform
DMF	N,N'-dimethylformamide
EtOH	Ethanol
FT-IR	Fourier Transform Infrared

	spectroscopy
KBr	Potassium Bromide
K_f	Theoretical Fluorescence Rate Constant
KOH	Potassium Hydroxide
M	Molar Concentration
MeOH	Methanol
UV-vis	Ultraviolet Visible Absorption Spectroscopy

Chapter 1

INTRODUCTION

Perylene diimide(PDI) is a broadly used Rylene chromophoric member in functional multichromophoric architectures due to their average oxidative and reductive potentials[1]. Considering PDI as a possible antitumor drugs which serves as telomerase inhibitors has greatly increased its scope of usage in biochemical and pharmacological purposes and also, the outsatnding applications of PDI in dye lasers, organic electronic devices, and light harvesting arrays, has greatly attarcted research [2]. PDI is the most studied n-type organic semiconductor with remarkable characteristics such as chemical and thermal stability, quick electron transportation, and high degree of electron acceptance. Synthesis had been done on PDI derivatives with pi-conjugation increasingly at the bay positions [3]. As regards to its electron transportation, the highest mobility was accounted for Tatemichi in the year 2006, who through his demonstrations by using annealing technique, an extremely arranged thin films appropriate to DMP FET showed a 2.1 $cm^2/(v.s)$ carrier mobility. LUMO energy level has been greatly lowered by bringing into play strong electron withdrawing pyrimidinyl ring in association with DMP [4]. Perylene polymers that exhibit solid-state emissions are promising prospects for photovoltaic applications and also to obtain a flexible polymer for self-organization with better solubility and varying photoluminescence properties, flexile sections are

incorporated of variable lengths into the backbone [5]. Perylene derivatives are used as dyes and pigments in coating and painting in organic chemistry. In addition, the stronger absorptives and emissions by PDI at the visible region, makes them a prime candidates for photoreceptors, photoconductors and lasser material applications and their usage in nonlinear optics field satisfies the search for organic compounds showing high nonlinear optical (NLO) absorption [6]. A remarkable use of PDI is as a sensitizer in a Dye-sensitized solar cells (DSSCs) [7].

PDI is applied as lacquers, fluorescent and near-IR dyes, optical switches, molecular switches, dye lassers, logic gates, and in reprographic processes. A great significant discovery was made on perylene derivatives by using PDI which was capable of performing a dual purpose by transporting both the electron and hole at the same time making it ambipolar [8-9]. Though much has been done based on the attractive properties of perylene derivatives, still yet much is to be done on improving the air stability of electron-transporting materials, solubility and aggregation in common solvents, the influence of the different organic inter-layers on the performance of the device, and on its lower solid state quantum efficiency which arises due to its self-quenching as a result of high concerntration of dye within the film [10]. Properties such as large charge carrier mobility, high thermostability, and good electron transport makes perylene derivatives suitable for applications in opto-electronics and excellent n-type semiconductors[11-14]. Most PDI applications were carried out on dye-sentisized solar cells up till date while conjugated perylene, perylene bisbenzimidazole i.e. conjugated perylene (CONPER) and PDI has accounted via thermal gravimetric analysis of a stability of 400ºC[15-17]. Fabrication of bilayered OPVs through vapor deposition has made low molecular weight derivatives of perylene to be examined as electron acceptors and further analysis has carried out on

PDI as active compounds in finger mark detection and living cell staining in biochemical applications[18-20]. PDI derivatives and PDI of tetracarboxylic acid shows great applications in industrial dyes[21-23]. Reaction of primary amines in m-cresol mix with isoquinline leads to the synthesis of a high yield symmetrical perylene diimides[24-25]. Solar cells made up of PDI and poly(3-hexylthiophene)(P3HT) shows lower efficiencies(0.2%) of external power conversion[26]. In 1992, successful encapsulations of the aqueous inner volumes of fluorescent liposomes was done by using dyes of perylene of high lipophilicity into the single phospholipidic bilayer of vesicles instead of using water soluble dye[27].

Perylene diimide derivatives among n-type oragnic materials have high molar absorption coefficients, awesome accepting characteriestics and a conduction through the π-π stacking axis[28]. Tang in 1986 successfully designed the first efficient oragnic bilayer photovoltaic cell by combining copper phthalocyanine and a perylene derivative[29]. Nowadays, assembly and characterization of organic-inorganic interfaces has been the area of intensive research though much is still to be done in the areas of selecting a proper cathode, proper modification of the cathode, device encapsulation to amend its stability and life time[30-31]. While high electron accepting abilities gives perylene imides an upper arm in transportations and opto-electronics, their low stability in organic solvents still stands as a hindrance. Perylene tetraesters such Tetraalkyls, is recently known as novel classes of self organized electron transporting stuffs[32-34]. The aim of this project is to synthesize a new perylene diimide and its monoimide for potential organic electronic and solar cell applications (Scheme 1).

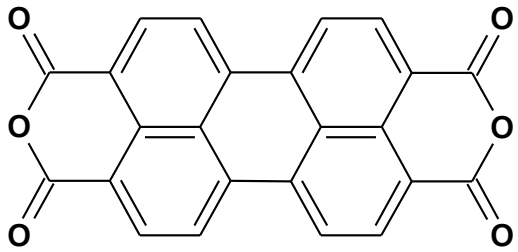

PDA

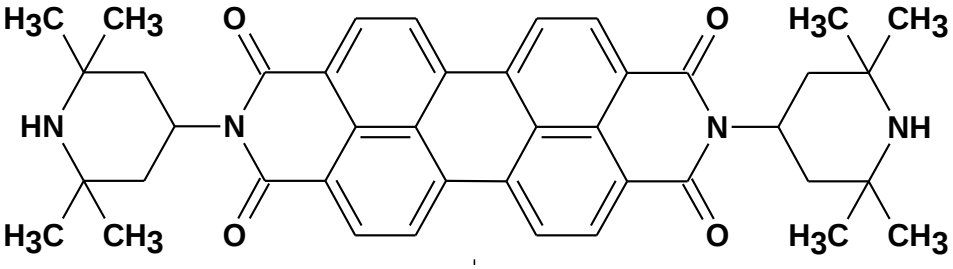

N,N’-Bis(2,2,6,6-tetramethyl-4-ppiperidinyl)-3,4,9,10-perylenebis-(dicarboximide)

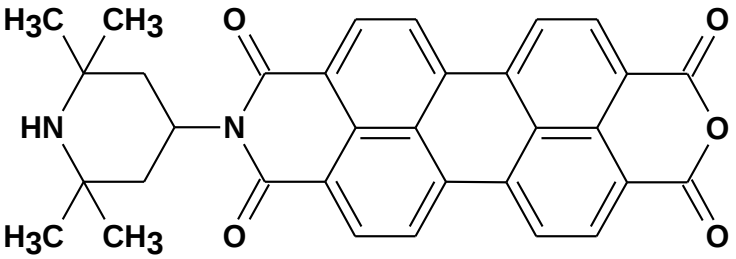

N-(2,2,6,6-tetramethyl-4-piperidinyl)-3,4,9,10-perylenetetracarboxylic-3,4-anhydride-9,10-imide

Scheme 1: General reaction routes for the synthesis

The synthesis was then followed by detailed characterization to explore the optoelectronic properties of perylene derivatives using UV-vis, and emission techniques. Structural characterization were performed by FTIR techniques.

Chapter 2

THEORETICAL

2.1 Types of Solar Cells

2.1.1 Classification based on Technology

Numerous types of solar cells (photoelectric cells or photovoltaic cells) exist today due to the advantageous future it sets forth being highly available and less expensive resulting from the application of an excellent work. With respect to technological approach, photovoltaics (PVs) can be classified into two main groups, that is; amorphous thin Film technology and Silicon crystalline technolgy.

2.1.1.1 Silicon Crystalline Technology

This type of PV is further divided into two major groups that is single crystalline solar cells and multi crystalline solar cells. It should be noted that most silicon solar cells (SSC) are made from wafers of silicon. These wafers are at times single or multi crystalline. Wafers made up of single crystalline are better as compared to multi-crystalline wafers with respect to manufacturing material but are costly as compared to the multi crystalline. Silicon crystalline has a well defined structure of crystals made up of well arranged atoms in pre-defined locations. Silicon crystalline predict and shows uniform behaviors but as a result of their careful processes and slow production involved, they remain the most expensive forms of silicon. Silicons form a quadruple linkage with neighboring atom.

The veritable arrangement of atoms of silicon in a single crystalline silicon develops a well defined pattern. An atom of silicon has four outermost electrons and therefore can used these outer most electrons in bonding with neighboring atoms. Single silicon crystal is developed as a huge cylindrical ingot giving rise to a solar cells which are semi squared or circular. Edges of a circular cell is usually cut-off to produce a semi squared cell in other to increase the total number of atoms used for the process in a rectangular module. Single-silicon PV cells are produced from single silicon crystals which are cylindrical through the application of the saw-cut method while multi-crystalline silicon PV cells are fabricated from recrystalized and ingot of melting silicon. Also, single-silicon PV cells has an operating efficiency of closed to15% while that of multi-silicon PV cells lies within the range of 12% and the later occupies about 90% of world's market on crystallined silicon [36]. Poly or multicrystalline silicon PV cells have become the core interest of most research centers and institutions or manufacturers due to its beneficial solubility of generating electricity [37].

2.1.1.2 Amorphous Thin Film Technology

The word 'amorphous' refers to non-crystalline substances made from gas depositions. Amorphous silicon can occur in its hydrogenated form. Early analysis of amorphous silicon ascertained that deposited-plasma amorphous silicon possessed a substantial percentage of atoms of hydrogen bonded into the structure of amorphous silicon. Materials' electronic properties were improved by these amorphous silicon atoms. Amorphous silicon is most popularly seen as an amorphous silicon which is hydrogenated (a-Si:H).

Advantages of a-Si:H over c-Si:

- Based on technology, it is relatively inexpensive and difficult for c-Si as to a-Si:H.
- a –Si:H draws a higher energy as likened to c-Si based on a known layer thickness, that is about 2.5 times.
- Films of a-Si:H needs a lesser material which is less expensive and has a lighter weight for its fabrication.
- a-Si:H deposits are made on numerous substrates such as roll-away categories, curve and flexible.

2.1.2 Conventional Solar Cells : Photovoltaic cells of First and Second Generations

With respect to depletion of energy sources which are non-renewable, a great interest was placed on renewable energy sources with great emphasizes made towards the production of solar cells. This search and zeal went on for decades from the first generation photovoltaics to present fourth-generation complexed of photovoltaic technology (PV). PV of first generation is based on basic stages made up of single layer p-n junction diodes and large area. It is maked basically of wafers of silicon and are known as wafer-based silicon solar cells. Its fabrication processes are costly per unit watts and are difficult, coventional solar cells made of silicon are prevalent in the commercialization of solar cells [39 – 40].

Thin Film deposited semiconductors and poly-junction photovoltaics cells materials constitute the second generation photovoltaics cells. These were made to meet up with the huge demand for energy by the industralized world and cost of production of first generation PV cells. These devices were made to be highly efficient. Thin Film semiconductors are made from various substances which possesses reduction in

material mass necessary for cell designing. PVs which are of second generation had a lower efficiency as likened to first generation PV cells but their lower fabrication cost gave an upper hand for further research [41-42].

In order to perceive the idea behind the third generation photovoltaics, it is necessary to comprehend the working the principle and theories of less complex photovoltaics. An extensive application of the technological aspect behind PVs leads to the production of large amounts of electricity for lighting homes, pumping water, powering electrical appliances, etc [37]. Semiconductor theories is used as a tool to better analyzed and eplain photovoltaic effects which is the cause of the conversion of radiations of electromagnetism into electricity [39-42].

2.1.2.1 Generation of Photons of Charge Carriers

Traditional photovoltaics are build by placing p- and n- type semiconductors in contact. a junction of p-n is made in silicon through the process of doping. These photons captured from the disclosed light motivated the flow of electrons from n–Si node to p-Si node or junction and this leads to the production of electricity. It should be noted that, three basic processes occurs when a photon strikes the surface of a silicon which determines the fate of the photon, viz;

i) The silicon surface will reflect the photon off.

ii) The silicon surface may absorb the photon which is as a result of a higher enegry possessed by the photon as compared to the band gap of the silicon atom. Should this occur, it will lead to the (a) pair electron-hole generations or (b) heat generation.

iii) The photon can pass via the silicon should it possess a lower energy as compared to the band gap of the atomic silicon.

What then becomes the fate of the photon should the second process comes to practice? Absorption of photon by an atomic silicon leads to excitation which involves the movement of an electron from its valence band to its conduction band. In its conduction band, it can move freely within the semiconductor. The formation of a hole also goes through the same mechanism when doping is done with a p-type material. A hole is created at the valence band when the electron leaves its location moving to a conduction band. Holes carry a positive charge since they indicate the absence or a lost of an electron. Should a missing covalent bond be present, neighbouring bonded electrons of atoms migrate to the empty holes creating another hole at the previous location thus making a hole to be mobile in the whole lattice.

What really is doping of semiconductors? Doping involves the addition of atoms of different electron numbers to obatin an unbalanced electron numbers in based materials (silicon, etc) for common semiconductors. After doping, the base material possesses excess electrons and therefore carries a negative charge while the based material possessing shortage of electrons becomes positively charge. Silicon doping can be obtained through ‘diffusion’ or ‘implantation of ion’ for negative charge by using Phosphorus (P) or Arsenide (As) and for positive charge by using Boron (B).

Taking a closer look at the doping of semiconductors either by diffusion or implantation of ions gives us a clue on how to reduce cost of production which is an extra advantage. Ion inplantation doping of silicon is carried out at room temperature while that of diffusion is done at higher temperatures. Energy is needed for dopant ionization when dealing with ion inplantation and it is a faster process of doping whereas a slower doping process is experienced with diffusion which is a chemical process though it is easy to manage and has a lower cost. A vivid conclusion can be

made that, charge carriers are created when absorbed photons leads to the formation of mobile pairs of electron-hole.

2.1.1.2.2 Charge Carrier Separation

For the production of electricity, separation of electron-hole union after its formation is of high necessity. This separation must occur and its migration must be in the direction of the electrodes. Two major ways of separation of charge carriers occurs in solar cells which are (a)- drifting of carriers of charges which involves driving by an electrostatic field generated in the whole device , and (b)- diffusion of charge carriers which involves movement from an area of high carrier concerntration potential to an area of lower carrier concerntration potential. The former is an outstanding model of separation of charge carriers in local solar p-n junction cells. What then happens in a non-local p-n junction solar cells (that is a third generation solar cell)? The previous involving the drifting, electrostatic fields are absent and its major type is separation through diffusion of charge carriers.

2.1.1.2.3 Conventional p-n Junction

Placing n-type and p-type silicon together leads to the creation of a junction known as junction of p-n. The interfecial boundary where the n and p semiconductors meet is known as its junction. On the above diagram, free electrons are shown with the aid of blue dots (n-type material) and red dots (p-type material) . In the zone of depletion, this formation results from the decalocalised electrons on the n-face and delocalised holes on the p-face behaving as wanderers on the surface. When these wanderers comes into contact, the delocalised electrons falls into the delocalised holes which leads to the cancellation of both the electron and the hole and zone depletion of moving charges.

Generally, this leads to minimal crystal lattice electrical imbalance. Due to the missing of an n-face, positive charges are being assigned to some electrons while holes filled by extra electrons located at the p-face will be assigned a negative charge. Power generation can never arise from electrical imbalance therefore creating a region without any free charge to counter balance a charge which finds itself in the depletion zone. With the present of this charge, the depletion zone exercises a force towards the free charges which pushes it towards its previous location on the junction. With this done, the depletion zone becomes clean with no free charge. At this juncture, a free will need extra force from a donor/acceptor atom to go across the depletion area. This depletion zone further acts as a barrier preventing flow of charges hence inhibiting current flow. An elternative power source e.g a battery maybe connected with its positive edge connected to the p-face and its negative edge connected to the n-face of the silicon. According to the theory of repulsion of like charges and attraction of unlike charges, the loose electrons will migrate towards the positive end of the power rootage and p-n junction while the loose holes will migrate towards the negative end of the power rootage. Current may pass across the diode should the holes and electrons received sufficient voltage to drive them across the depletion area. Such a diode is forward-biased. Should a reverse applications be made in the designing, unlike charges would attract each other, that is attaching a positive end to an n-type silicon and a negative end to a p-type silicon. N-type silicon (negatively charge electron) will be pulled to the positive end while the p-type silicon (positively charged holes) will move towards the negative end.

2.1.1.2.5 Factors influencing Solar Cells' Efficiency

Efficiency is the most apparent measure that characterizes solar cells. To look at factors which influences the efficiency of SCs, we have to first take a look at important parameters that makes us to understand the performances of PVs. These include; a)- Fill Factor (FF): the voltage from a SC is called an open circuited voltage while short circuit current is its maximum current. FF is often defined as the proportion of ultimate SC power to V_{oc} and I_{sc} products. FF is directly proportional to the performance of the SC, b)- Efficiency: it is the proportion of SC energy output to sun's energy input. The SC temperature, intensity and spectrum of the incident sunlight are determinants of SC efficiency. Efficiency is further analysed as the proportion of incident power changed to electricity and represented mathematically as follows:

$$\mathbf{P_{max.} = V_{oc}\, I_{sc} FF}$$

$$\eta = \frac{\mathbf{Voc\ IscFF}}{\mathbf{Pm}}$$

Where P_m is the ratio of the maximum power point, V_{oc} represents an open circuit voltage, Isc denotes a short circuit current, η is energy conversion efficiency and FF is the fill factor.

Critical factors affecting solar cells efficiency includes;

Temperature of the cell:

An increase in temperature causes the shrinking of the band gap of the intrinsic semiconductor and decrease of the V_{oc} as a result of the dependency of the voltage temperature of the p-n junction as shown in $^{q}/_{kt}$ i.e. the diode factor. SCs possesses

negative V_{oc} temperature coefficients denoted as ß. When charge carriers are delivered at a lower potential, a lower power output is obtained asiging same photocurrent. Application of the rule in the calculation of fill factor, reducing V_{oc} output in a littler maximum power theoretically,

$P_{max} = V_{oc}$ X I_{sc} allocating the same units for I_{sc} . An inherent factor of modules made from crystalline silicon is temperature. As teperatures falls, voltages increases in modules and vice versa. Temperature adjustment effect is very necessary in system derating calculations.

Conversion Efficiency of Energy

Eta or η is energy conversion efficiencies of solar cells which is the percentage of light absorbed that has been converted to electrical energy and gathered when an electrical circuit is attached to a SC. Mathematically, η is analysed through the application of P_m(point of maximum power) dividing it by E (irradiance light input measured in W/m^2) and A_c (SC total area surface measured in m^2).

$$\boldsymbol{\eta = \frac{Pm}{Ac\ Ex}}$$

We still obtain lower energy conversions and thus this raises eye brows on required energies for production of cells versus energies harvested demanding larger surface areas for optimum insulations. Two methods are applied widely as to augment energy conversion efficiencies by decreasing incident light reflections of SCs. Primarily, incident light reflections with antireflection coatings and secondly with textured surfaces of optical incident lights confinement. Enhancement of spectral sensitivities of photodiode of silicons are significantly altered by the light wave length transformations from deep ultraviolet and via visible region.

Maximum Power Point Tracking

Presently, transformation efficiencies of electricities of SCs are very low closed to 14% and thus requires improvement on SCs efficiencies via various methods. One of these methods is MPPT (maximum power point tracking). MPPT functions with direct current to direct current of higher efficiencies converters which shows a suitable and optimal power output. Current generated from photons, I_L is adequate to short circuit current production, V = 0. V_{oc} (I = 0) is easily obtained. Power generation is zero under open or short circuits. Conversion devices produces P (maximum power) at characteristic points. Also FF can be defined as;

$$\mathbf{ff} = \frac{\mathbf{Pmax}}{\mathbf{Voc}} = \frac{\mathbf{VmIm}}{\mathbf{VocIl}}$$

V_m and I_m are current at maximu power point. PV cell arrays' output voltages maybe extremely low causing a little change on current output due to changes in voltages. PV cell arrays show similarity with constant sources of current when voltages beyond critical values keep increasing, sharply the current drops making the PV cell arrays alike to constant sources of current. Due to the constant increase in the voltage output, the power output arrives a peak or its maximum known as maximum power point. The basic principle of a tracker of maximum power is to manage equivalent load from the array of PV cell and readjust the array's working point on the PV cell so as maximize the working power of the PV cell array at fluctuating radiant intensities and temperatures at the peak of maximum power point.

2.1.1.3 Third Generation PVs (Organic Solar cells)

Due to enormous difference in bonding system in third generation PVs as to first and second generation PVs, OPV(third generation PVs) do not separate its generation of

photo-charge carriers by the normal traditional p-n junction. Due to their ease in production, low cost and mechanical flexibility, they have gain world demand [42-54, 19]. An enormous possible solar inventions are being inscribed in third generation PVs which includes; dye-sentization of PVs, cells of nanocrystalline, polymeric PVs, and cells of photoelectrochemical products. Conversion of power in OPVs has greatly increased from 0.001 percent around 1975 to a unit percentage in 1986 and lately to about 5.5 percent in the early 2006 [17]. Due to its potentials, future growth in efficiency and commercialization can be attain. Their strain optical characteristics and fabrication makes them excellent alternatives of conventional PVs.

2.1.1.3.1 Designing principle

Designing characteristics of OPVs can be represented diagramatically as follows;

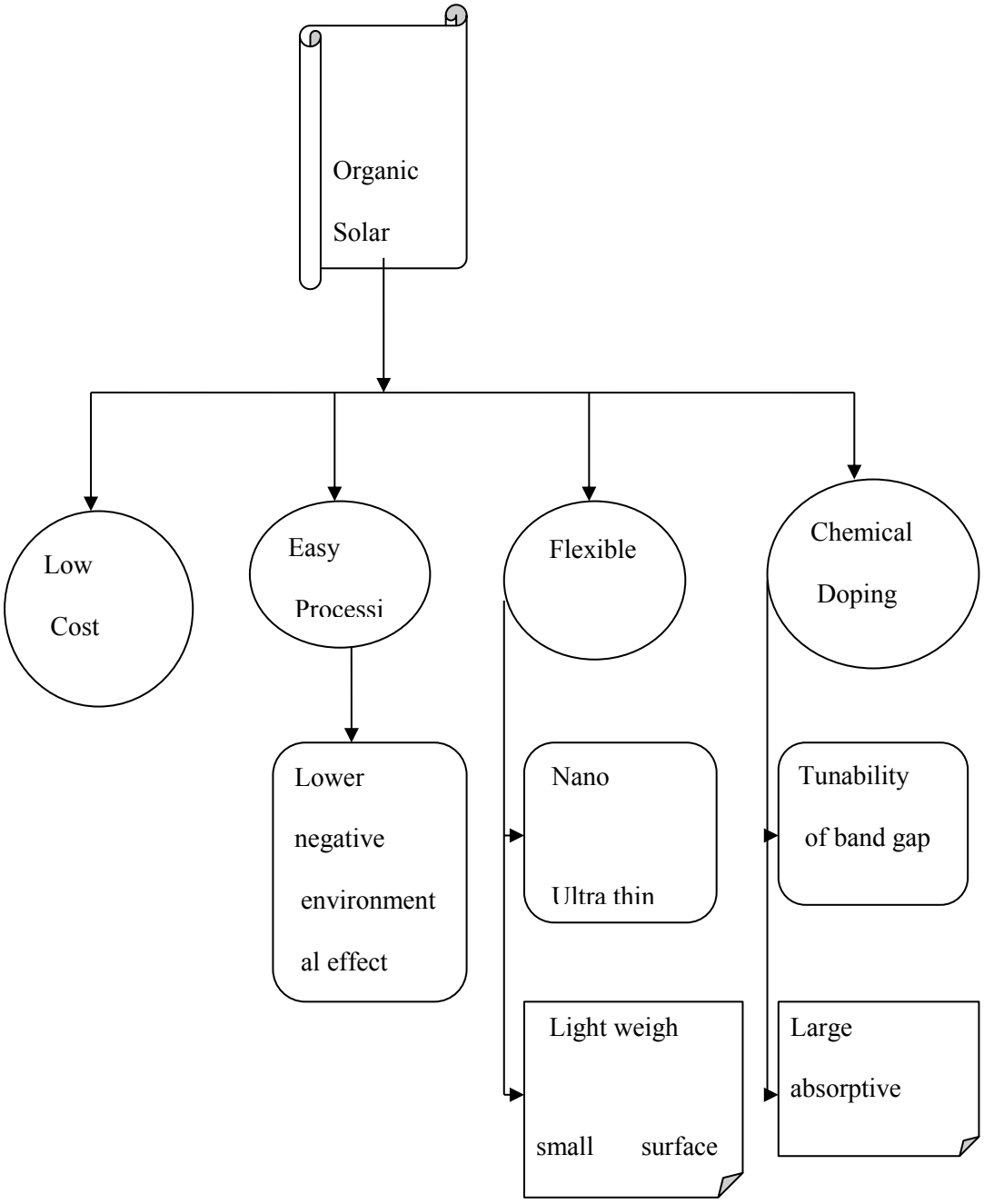

Figure 2.3: Leading designing characteristics of OPVs

2.1.1.3.2 Charge Transport Mechanism – Exciton Concept

Mechanism of quantum wave-length and orbitals of π-bonding determines the charge transport system in SCs. Conjugated materials are made up of overlapping organic semiconductors. As earlier talked about on valence bands and conduction in established (conventional) PVs will be attributed to LUMO/HOMO. MO (Molecular orbital) is form from p-orbital interactions with the carbon atoms of the conjugate backbone. This interaction leads to the creation of anti-bonding- π^* and bonding- π molecular orbital making OPVs to show a fundamental difference in their mode of functioning. Band gaps created results from the energy difference between the two levels and this determines the optical characteristics of the substance. Van der Waals are weak intermolecular forces that holds organic substances together via a covalent intra-molecular bonding while in conventional PVs, same bonding occurs but substances are held together by powerful covalent bonds which creates a three dimensional structures which emerges to electronic bands hence semiconducting characteristics. Bands aren't form since all electronic states are situated on single molecules. Exciton is a powerful electron-hole charged pair resulting from a coulombical bounding due to excitation of organic substances by photons. Generation of charge separation carriers don't emerge from light absorption since excitons don't break down into pairs of charges due to their strong bounding. The capability of carriers of charges to move from one molecule to the other determines the transportation of charges. This form of transportation system is known as a hopping. HOMO and LUMO energy gaps determine the hopping of carriers of charges from one molecule to another. The mobility of the carriers relies on the copiousness of the same levels of energy for holes or electrons to migrate to and fro

leading to demarcation of regions with higher hopping potentials and others with lower hopping potentials [56-58].

2.2 Solar Cell Materials

Common PVs may be tabulated as follows:

Table 2.1: common solar cell materials.

Single crystalline	Polycrystalline (Thin films)	Organic
Polycrystalline silicon GaAs Amorphous silicon Single crystalline	CIS CdTe	Polymers Perylene Napthalene, etc

2.2.1 Perylene Dyes: Promising n-type Organic Semiconductors

With respect to Gratzel, DSSCs are the only third generation PVs which can dispute solid-state inorganic junction appliances [59]. An electrolyte, gel, solid, or liquid is used in replacing contact phases of semiconductors leading to the creation of an electrochemical photo-cell. Light absorbers (sensitizers) substances and a nanocrystalline morphological semiconductor with wide band gap association leads to optical absorption and separation processes of charges occurrence. TiO_2 (Mesoporous oxide) commonly used in DSSCs is made up of a section of nano-particles which are blended together to promote electronic conductivity in the core of DSSCs. ITO is a conductive layer which serves as a deposition surface for TiO_2 . Placing the electrolyte in contact with the dye on top of the film of semiconductor. Injection occurs when the dye is excited by irradiations of electrons into

semiconductor conduction band where it comes in contact with the anode of the cell via diffusion. When the redox electrolytes come in union with a dye, regeneration of electronic dye occurs through donation. This often takes place via a couple of iodide/triiodide in an organic solvent. At the level of the counter electrode, triiodide undergoes reduction while the movement of an electron towards the counter electrode from the anode shuts down the circuit. The differences experienced between the electrolyte's redox potential and the solid TiO_2 electron at its Fermi level is equal to the total voltage rendered [59-60]. n-type organic substances made are in a limited number as compared to p-type organic semiconductors. This disparity arises as a result of the difference in designing in the two semiconductors. Molecular design encounters difficulty when designing electron deficient conjugated polymers (n-type) as to designing its electron rich counterpart (p-type). Hapless air stabilities, difficulties in synthesis and hapless solubility are the draw backs of huge n-type semiconductor fabrication. With such complexities arises a huge demand for improved performances and improved durability of organic substances. Hydrocarbon based polymeric compounds are often used in n-type PVs possessing substituent which are electron withdrawing groups e.g. nitro and cyano groups and other renown naphthalene, fullerene, and perylene derivatives[61-62].

2.2.2 p-type Organic Semiconductors

A huge number of electron rich semiconductors (p-type) have been studied and characterized. Acenes which include pentacene, and oligomers such as poly thiophenes and oligo thiophenes are well renowned p-type semiconductors. Through doping at the conjugated π orbitals, these substances become conductive through the addition or removal of electrons. Π conjugated molecules contain higher HOMO units and shows characteristics of donating electrons. Conduction of electrons

(electrical conductivity) results electron delocalization along the backbone of the polymer. This leads to the development of a fill valence band π system known as a synthetic metal. Other optical characteristics are also exciting not only conductivity which is as a result of delocalization. In semiconductors doping is carried out at lower stages while in conducting polymeric compounds, it is done at a higher level. Partially oxidizing a polymer with an oxidant chemically or electrodes which leads to HOMO (p orbital) depopulating with holes injection is known as p-doping whereas n-doping is partially reducing a polymer chemically by a reductant or electrodes leading to electron injection in the LUMO (anti-bonding p system). Bipolaron is a charge unit created when a conjugated π system gains (n-doping) or loses (p-doping) an electron. Conductivity of polymer arises due to the constant migration of the bipolaron in an up and down movement within the polymer. N-doping i.e. reduction of polymer conductivity is less renowned as compared to the p-doping [61-62].

Chapter 3

EXPERIMENTAL

3.1 Reagents and Equipments

3.1.1 Reagents

4-amino-2, 2, 6, 6-tetramethyl piperidine, isoquinoline, m-cresol, and perylene-3, 4, 9, 10-tetracarboxylic acid were obtained from Aldrich, a German Company. Basic organic solvents were not distillated and distillation was done with respect to procedures found in standard literature. As regards spectroscopic analyses, spectroscopic solvents which are of pure grade were used after Argon gas bubbling in order to remove dissolved oxygen from solvents.

3.1.2 Instruments

Ultraviolet Absorption spectra

Measurements of ultraviolet spectra in liquids were evaluated with the use of a Varian Cary-100-Spectrometer.

Infrared Spectrum

Infrared spectra were acquired from a JASCO FT-IR-6200 Spectrometer by using solid KBr pellets.

Emission Spectra

Varian Cary Eclipse Fluorescence spectrophotometer was used to analyze the emission spectra of the synthesized compounds. All emission spectra were carried out at λ_{exc} = 485nm.

3.2 Methods of Synthesis

The aim of this Thesis is to synthesize a novel perylene monoimde from its diimide for potential organic electronics and solar cell applications. The synthesized perylene monoimide will be easily bind to titanium dioxide (TiO_2) for required applications. In this project, N,N'-Bis(2,2,6,6-tetramethyl-4-piperidinyl)-3,4,9,10-perylenebis (dicarboximide), (PPDI). Then N-(2,2,6,6-tetramethyl-4-piperidinyl)-3,4,9,10-perylenebis-(dicarboximide), (PPMI) was synthesized from the synthesized PPDI. Scheme 3.1 below shows the overall route for the synthesis of PPMI.

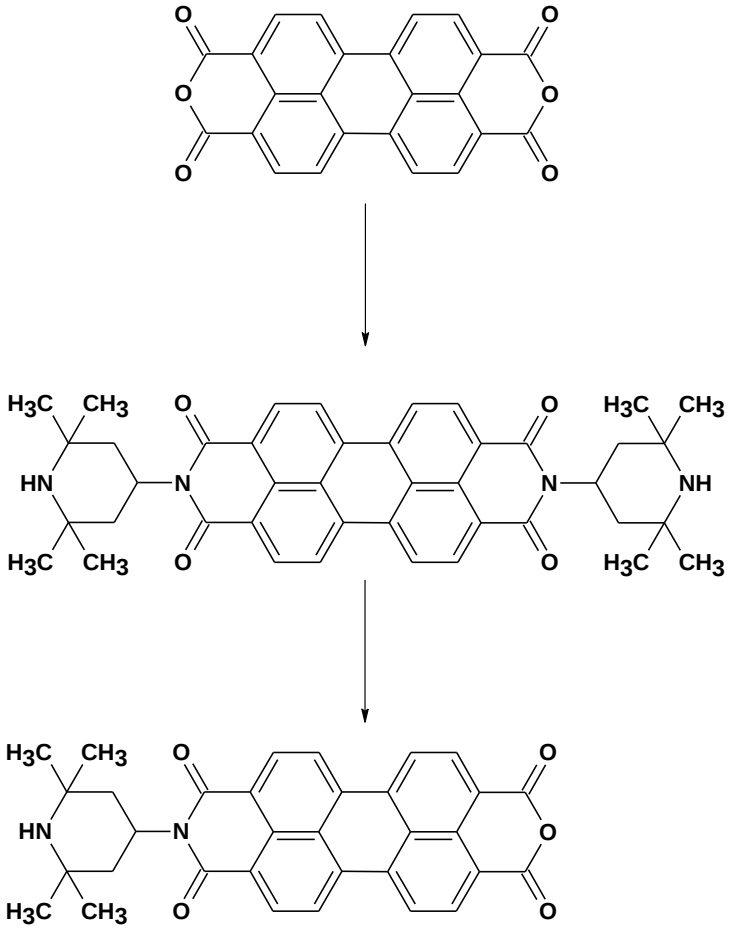

Scheme 3.1: Synthetic route of PPMI.

As it is shown scheme 3.2, in first step, a suspension of 4-amino-2,2,6,6-tetramethyl piperidin and perylene dianhydride (PDA) in the presence of m-cresol and isoquinoline reacted with the PDA to yield the PPDI was synthesized.

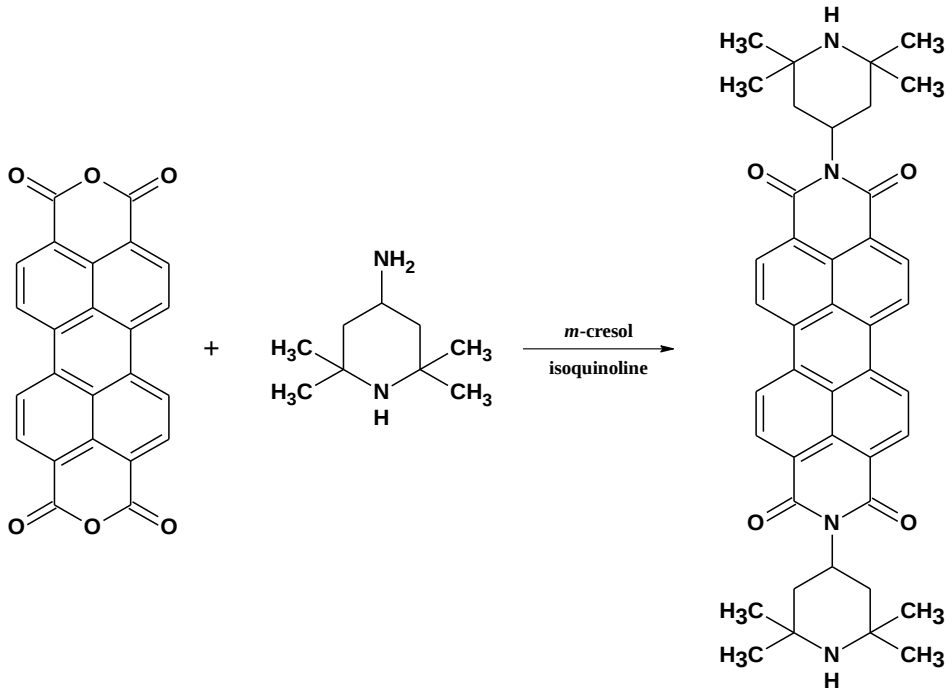

Scheme 3.2: Synthesis of PPDI (Spectroscopy Letters, 34(5), 605-614 (2001).

In the second step, which was the final step, PPDI was converted to PPMI in the presence of potassium hydroxide (KOH), Isopropanol, and water as it is shown in scheme 3.3.

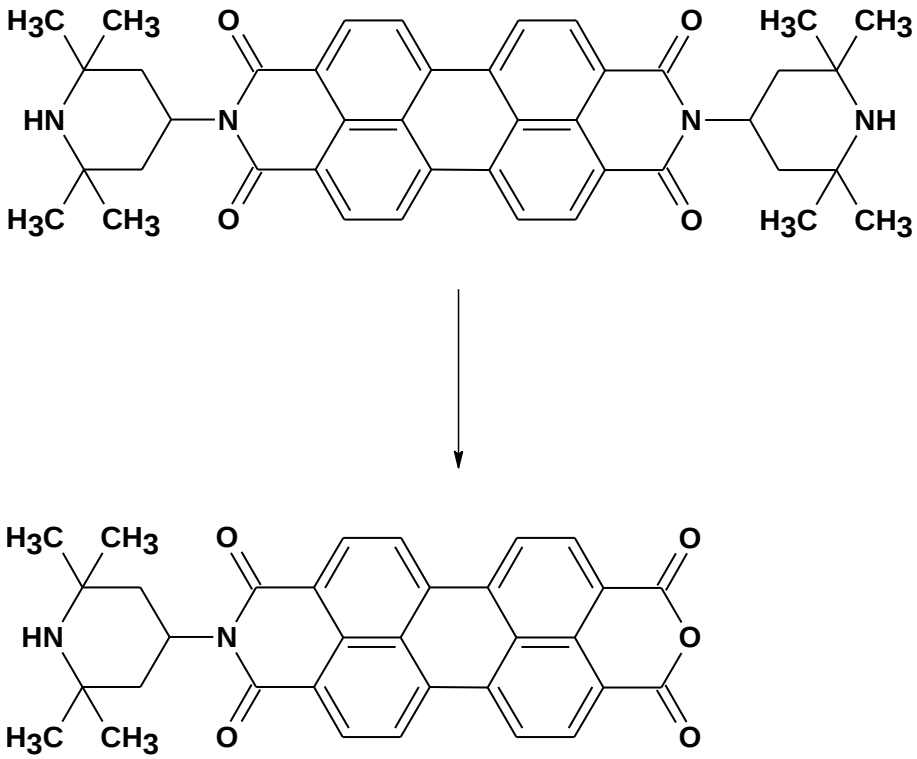

Scheme 3.3: Synthesis of N-(2,2,6,6-tetramethyl-4-piperidinyl)-3,4,9,10-perylenebis-(dicarboximide), (PPMI).

3.2.1 Synthesis of N,N'-Bis (2,2,6,6-tetramethyl-4-piperidinyl)-3,4,9,10-perylenebis-(dicarboximide) (PPDI)

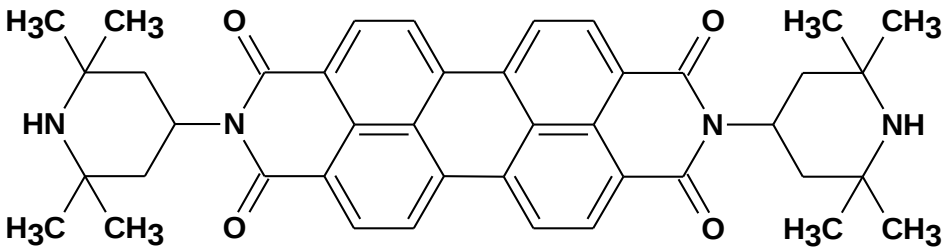

A suspension of PDA (1.007g, 2.57mmol) and 4-amino-2,2,6,6-tetramethylpiperidine (1.09/ml, 6.36/mmol) in m-cresol (40ml) and isoquinoline (4ml) were reacted with Argon (Ar) atmosphere in a 3-necked round bottom flask. The reaction mixture were heated at 80°C for 1hrs, at 120°C for 1hrs, at 150°C for 2hrs, at 180°C for 3hrs, and 200°C for 3hrs. The end of the heatings, the reaction mixture was poured into acetone (250ml) for precipitation and precipitates was filtered off via suction filtration. The crude product was purified by soxhlet for 16hrs and dried in vacuum oven for 24hrs at 100°C.

Yield: 97.68% (1679g); **Color:** red

FT-IR (KBr, cm^{-1}): v = 3428, 3289, 2962, 2928, 2860, 1686, 1651, 1594, 1576, 1463, 1404, 1341, 1258, 1171, 1127, 1014, 854, 810, 746, 648, 484.

UV-Vis (CHL) (λ_{max}/nm (ε_{max}, 1/L.mol^{-1}.cm^{-1}): 492 (87000), 526 (138000), 550 (78000), 581 (58000).

Fluorescence (CHL) (λ_{max}/nm (ε_{max}/ L.mol^{-1}.cm^{-1}): 536, 577, 624. Φ_f =0.11.

Reference: Spectroscopy Letters, 34(5), 605-614 (2001).

3.2.2 Synthesis of N-(2,2,6,6-tetramethyl-4-piperidinyl)-3,4,9,10-perylenetetracarboxylic-3,4-anhydride-9,10-imide (PPMI)

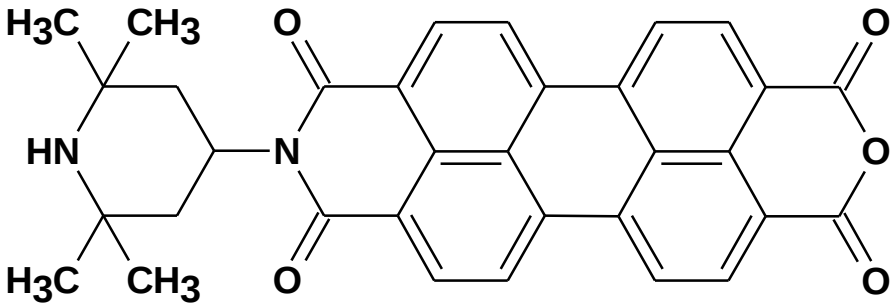

In to a 2-necked round bottom flask N,N'-Bis-(2,2,6,6-tetramethyl-4-piperidinyl)-3,4,9,10-perylenebis-(dicarboximide) (PPDI) (1.001g, 1.495 mmol), in isopropanol (70ml), water (10ml) and KOH (4.195g, 74.77 mmol) were stirred under room temperature for 30 minutes. The reaction mixture was then refluxed for 24 hrs and poured into 100mL of dilute HCl. The precipitate was filtered off and washed with water. The crude product was re-suspended of in 100 mL of 5% KOH and stirred for 30mins. The precipitate was filtered off and the product was washed with dilute HCl.The product was purified by soxhlet in Chl. Finally, the pure product was dried at 100°C under vacuum for 24hrs.

Yield: 78%; **Color:** reddish-brown.

FT-IR (KBr, cm^{-1}): v = 3274, 2484, 2421, 1762, 1734, 1700, 1656, 15598, 1413, 1127, 1060, 1038, 1258, 883, 811, 701, 671, 605.

UV-Vis (CHL) λ_{max}/nm (ε_{max}, $L.mol^{-1}.cm^{-1}$): 489 (82000), 521 (92000), 547 (59000), 574 (45000).

Fluorescence (CHL) λ_{max}/nm: 536, 577, 624.

3.3 General reaction mechanism for Perylene diimide Synthesis

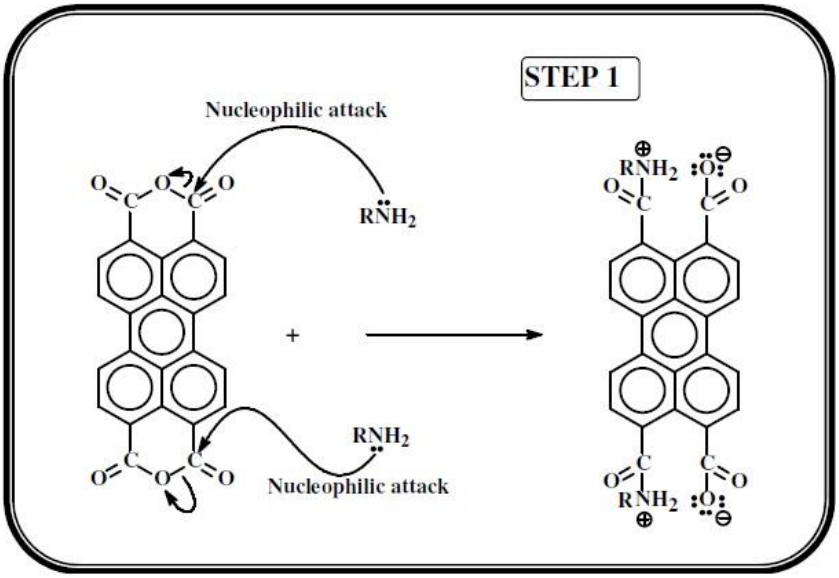

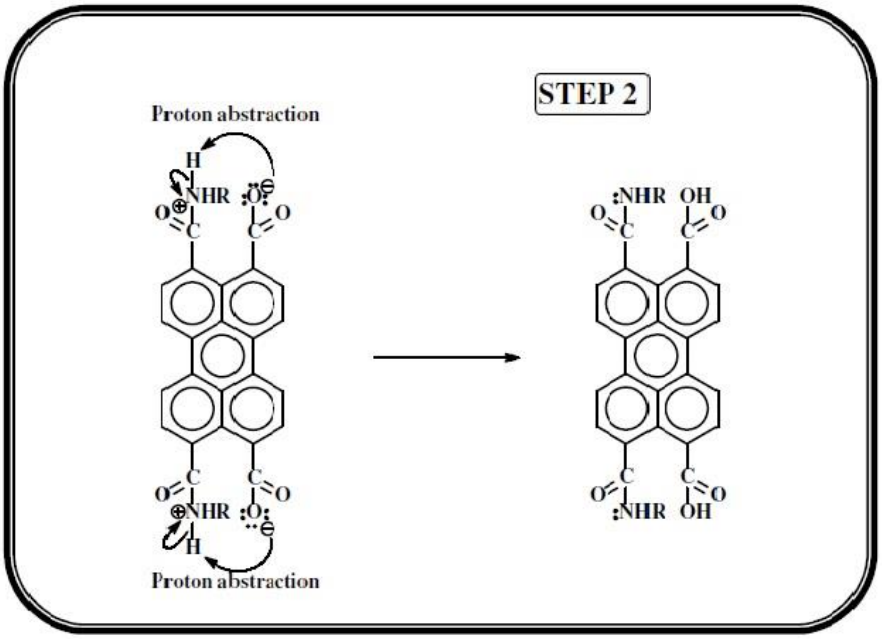

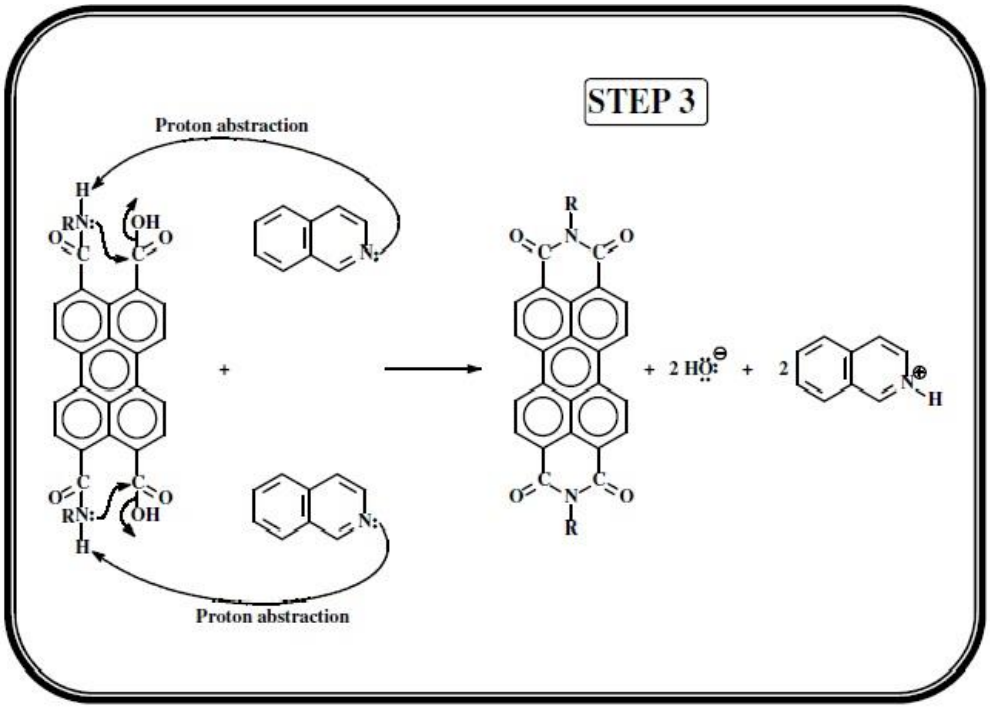

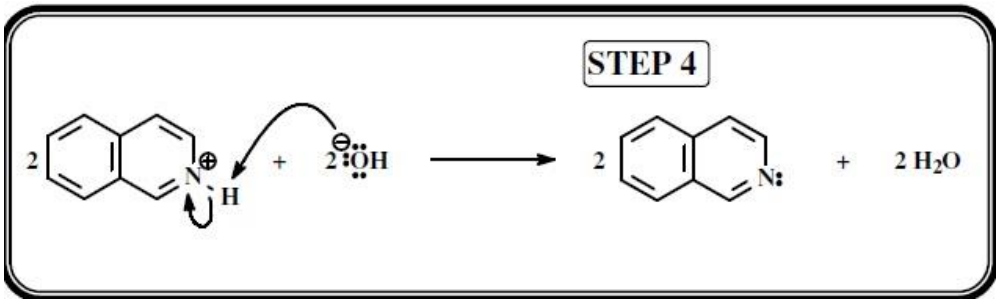

Source: Bodapati, J., B., 2011

Chapter 4

DATA AND CALCULATIONS

4.1 Calculations of Fluorescence Quantum (Φ_f)

Fluorescence quantum yield is the ratio of photons absorbed to that of photons emitted via fluorescence. Its mathematical formula is as follows;

$$\Phi = \frac{Total\ amount\ of\ photons\ absorbed}{Total\ amount\ of\ photons\ emited}$$

Fluorescence quantum yield is a significant parameter used to illustrate the characteristics of molecules if they emit the light absorbed or if they deactivate the light absorbed through heat. Williams et al. are well-known comparative method used in the calculation of Φ_f of a substance with the use of standard samples which are characterized with a known Φ_f [63]. Assumptions are made that, at same excitation wavelengths, both the standard and the test solution compounds had absorbed equal amounts of photons. Ratio of integrated fluorescence intensity of two solutions of compounds gave the quantum yield value. The equation below is used to calculate the Φ_f of the unknown compound in the presence of a standard compound with known Φ_f.

$$\mathbf{\Phi_u = \frac{A_{std}}{A_u}\ X\ \frac{S_u}{S_{std}}\ X\ \left[\frac{n_u}{n_{std}}\right]^2\ X\ \Phi_{std}}$$

Φ_u = Fluorescence quantum yield of unkown

A_{std} = Absorbance of the reference at the excitation wavelength

A_u = Absorbance of the unknown at the excitation wavelength

S_{std} = The integrated emission area across the band of reference

S_u = The integrated emission area across the band of unknown

n_{std} = Refractive index of reference solvent

n_u = Refractive index of unknown solvent

Φ_{std} = Fluorescence quantum yield of reference. [31, 32]

Fluorescence quantum yields of the perylene dye synthesized were calculated through the application of N,N'-bis(dodecyl)-3,4,9,10-perylenebis(discarboximide) as a reference compound and its $\Phi_f = 1$ in CHL [32]. All the dyes (perylene) used in the Φ_f calculations were excited at the wavelength of λ_{exc} = 485 nm.

Φ_f Calculation of PPMI in CHL

Referencing is N,N′-bis(dodecyl)-3,4,9,10-perylenebis(discarboximide) [32].

Φ_{std} : 1 in chloroform

A_{std} : 0.1055

A_u : 0.1083

S_u : 289.46

S_{std} : 4129.22

$\Phi_f : \frac{0.1055}{0.1083} X \frac{289.46}{4129.22} X \left[\frac{1.446}{1.446}\right]^2$ X 1

Φ_f : 0.07

Table 4.1 Fluorescence Quantum Yields of PPDI and PPMI in CHL

Compound	**Solvent**	Φ_f
PPDI	CHL	0.11
PPMI	CHL	0.07

4.2 Calculations of Molar Extinction Coefficients (ε_{max})

Molar extinction coefficients of the synthesized perylene derivatives were calculated according to Beer-Lambert's law, that is;

$$\varepsilon_{max} = \frac{A}{cl}$$

Where,

ε_{max} : Molar extinction coefficient in $L^{-1}cm^{-1}$ at λ_{max}

A : Absorbance

c : Concentration in $mol.L^{-1}$

l : path length in cm

ε_{max} Calculation of PPMI in CHL

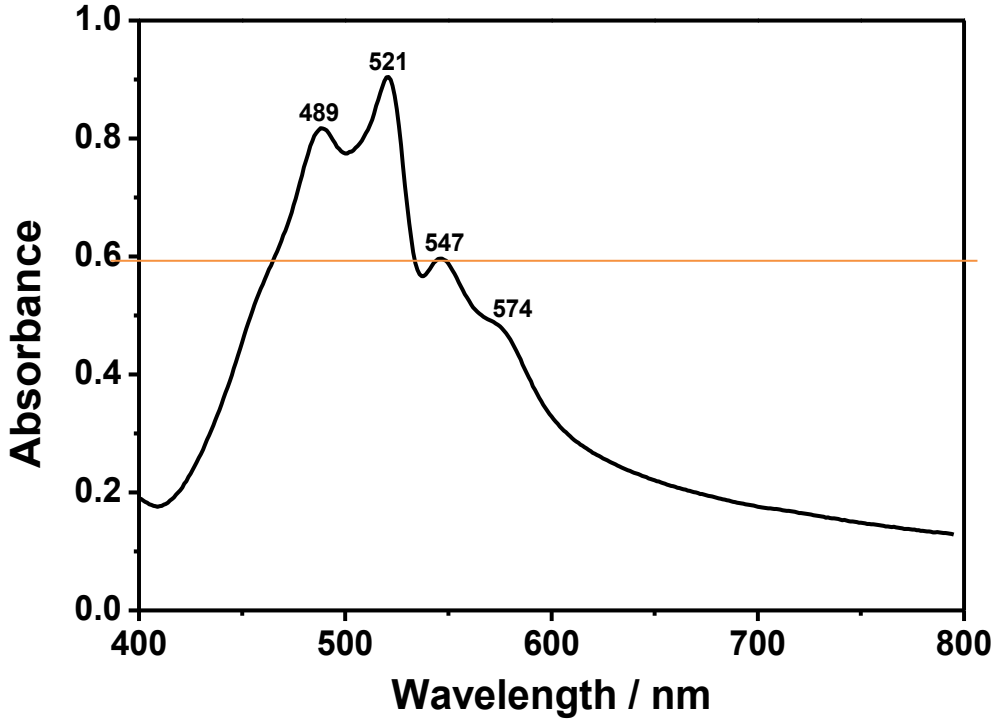

Figure 4.1: Absorption Spectrum of PP-PMI in CHL at a concentration of 1 x 10^{-5} M.

According to the absorption spectrum of PP-PMI at 1 x 10^{-5} M conc. (Figure 4.1), its absorbance is 0.60 at a maximum wavelength of, λ_{max} = 547 nm.

$$E_{547} = \frac{0.60}{1 \text{ x } 10^{-5} \text{ M X } 1 \text{ cm}} = 60000\ L.\text{mol}^{-1}.\text{cm}^{-1}$$

ε_{max} for PP-PMI is equal to 49000 L.mol^{-1}.cm^{-1}

Table 4.2 below shows the molar absorptivities of all the compounds calculated.

Table 4.2: Molar absorptivities of PP-PDI and PP-PMI in different organic solvents

Compound	**Solvent**	**Conc. (M)**	**A**	**λ_{max} (nm)**	**ε_{max} ($M^{-1}cm^{-1}$)**
PP-PDI	DMF	1×10^{-5}	0.9	549	90000
PP-PMI	DMF	1×10^{-5}	0.31	544	31000
PP-PDI	CHL	1×10^{-5}	0.67	550	67000
PP-PMI	CHL	1×10^{-5}	0.60	547	60000
PP-PDI	MeOH	1×10^{-5}	0.74	547	74000
PP-PMI	MeOH	1×10^{-5}	1.34	517	134000

4.3 Calculations of Half-width of the Selected Absorption ($\Delta\bar{\nu}_{1/2}$)

The half-width maximum of the assigned wavelength is the full width at half width maximum.

Formula used in the calculation of $\Delta\bar{\nu}_{1/2}$ is stated below.

$$\Delta\bar{\nu}_{1/2} = \bar{\nu}_1 - \bar{\nu}_2$$

Where

$\bar{\nu}_1$ and $\bar{\nu}_2$: are the frequencies from the absorption spectrum measured in cm^{-1}

$\Delta\bar{\nu}_{1/2}$: half-width of selected maximum absorption measured in cm^{-1}.

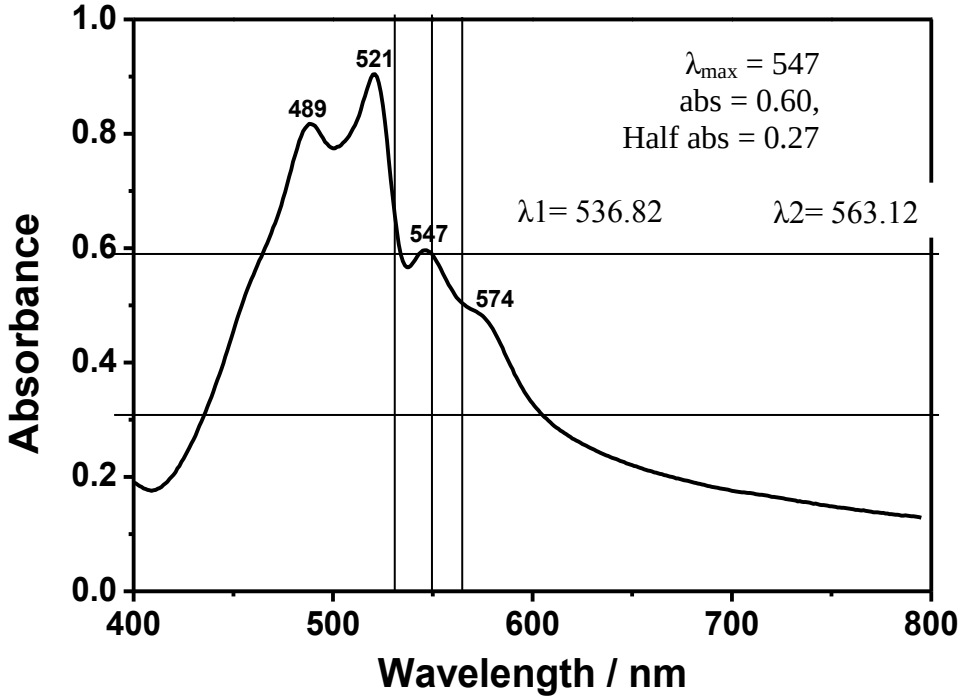

Figure 4.2: Absorbance spectrum of PPMI in CHL at a concentration of 1 x 10^{-5} M.

According to the above Figure 4.1,

λ_{max} = 547 nm

half-width absorption = 0.27

λ_1 = 536.82 nm

λ_2 = 563.12 nm

λ_1 = 536.82 nm x $\frac{10^{-9}m}{1\ nm}\ x\ \frac{1\ cm}{10^{-2}m} = 5.368\ x\ 10^{-5}\ cm$

$\bar{\nu}_1 = \frac{1}{5.407\ x\ 10^{-5} cm} = 18628.21\ cm^{-1}$

λ_2 = 563.12 nm x $\frac{10^{-9}m}{1\ nm}\ x\ \frac{1\ cm}{10^{-2}m} = 5.631\ x\ 10^{-5}\ cm$

$\bar{\nu}_2 = \frac{1}{6.3333\ x\ 10^{-5} cm} = 17758.204\ cm^{-1}$

$\Delta\bar{\nu}_{1/2} = \bar{\nu}_1 - \bar{\nu}_2 = 18628.21\ cm^{-1} - 17758.204\ cm^{-1} = 870.02\ cm^{-1}$

A compound's theoretical radiative lifetime is calculated through the estimation of half-widths of its absorptive spectra. Same mathematical analysis as shown above

were applied for the calculation of the various half widths and tabulated as below on Table 4.3.

Table 4.3: Half-widths of compounds of PP-PDI and PP-PMI selected absorptions obtained.

Compound	Solvent	λ_{max} (nm)	λ_1 (nm)	λ_2 (nm)	$\Delta\bar{\nu}_{1/2}$ (cm^{-1})
PP-PDI	CHL	550	539.45	568.38	943.54
PP-PMI	CHL	547	536.82	563.12	870.02
PP-PDI	DMF	549	535.52	563.16	916.49
PP-PMI	DMF	544	534.19	568.38	1126.07
PP-PDI	MeOH	547	518.41	551.29	150.48
PP-PMI	MeOH	517	492.05	542.08	1875.68

4.4 Calculations of Theoretical Radiative Lifetimes (τ_0)

The theoretical radiative lifetime of a molecule is measured in the absence of non-radiative transitions. The theoretical radiative lifetime is calculated as follows [65].

$$\tau_0 = \frac{3.5 \text{ X } 10^8}{\bar{\nu}_{max} \text{ X } \varepsilon_{max} \text{ X } \Delta\bar{\nu}_{1/2}}$$

Where

τ_0 : Theoretical radiative lifetime in ns

$\bar{\nu}_{max}$: Mean frequency of the maximum absorption band in cm^{-1}

ε_{max}: The maximum extinction co-efficient in L. mol^{-1} cm^{-1} at a maximum absorption wavelength, λ_{max}

$\Delta\bar{\nu}_{1/2}$: Half-width of the selected absorption in units of cm^{-1}

Theoretical Radiative Lifetime of PP-PMI:

With the application of deduced values of PP-PMI's half-width and molar absorptivity of assigned absorptions, the theoretical radiative lifetime was calculated in CHL.

From Figures 4.1 and 4.2,

λ_{max} = 547 nm

λ_{max} = 547 nm X $\frac{10^{-9}m}{1\ nm}\ X\ \frac{1\ cm}{10^{-2}\ m} = 5.47\ X\ 10^{-5}\ cm$

$\bar{\nu}_{max}$ = $\frac{1}{5.47\ X\ 10^{-5}\ cm} = 1.82\ X\ 10^{4}\ \ cm^{-1}$

$\bar{\nu}^2_{max} = (18281.54\ cm^{-1})^2 = 3.34\ X\ 10^{8}\ cm^{-2}$

Then the theoretical radiative lifetime is deduced as follows;

$\boldsymbol{\tau_0} = \frac{3.5\ X\ 10^{8}}{\bar{\nu}^2 max\ X\ \varepsilon_{max}\ X\ \Delta\bar{\nu}_{1/2}} = \boldsymbol{\tau_0} = \frac{3.5\ X\ 10^{8}}{3.34\ X\ 10^{8}\ \ X60000\ X870.006}$

$\boldsymbol{\tau_0}$ = 2.01 X $10^{-9}s$

$\boldsymbol{\tau_0}$ = 2.01n*s*

In a similar manner, the theoretical radiative lifetime of all the synthesized compounds at different solvents were calculated and reported in Table 4.4.

Table 4.4: PP-PDI and PP-PMI theoretical radiative lifetimes.

Compound	**Solvent**	**λ_{max} (nm)**	**ε_{max} ($M^{-1}cm^{-1}$)**	**ν^2_{max} (cm^{-2})**	**$\Delta\nu_{1/2}$ (cm^{-1})**	**τ_0 (s)**
PP-PDI	CHL	550	90000	330578512.4	943.54	1.24×10^{-8}
PP-PMI	CHL	547	31000	334214545.7	870.02	3.88×10^{-8}
PP-PDI	DMF	549	67000	331783902.5	916.49	1.72×10^{-8}
PP-PMI	DMF	544	60000	337910899.7	1126.07	1.53×10^{-8}
PP-PDI	MeOH	547	74000	334214545.7	150.48	$9.40 X 10^{-8}$
PP-PMI	MeOH	517	134000	374126881.4	1875.68	3.72×10^{-9}

4.5 Calculation of Theoretical Fluorescence Lifetime (τ_f)

Fluorescence lifetime is the average time of a molecule that remains at the excitation state before fluorescence. The theoretical fluorescence lifetime can be calculated from the following equation,

$$\tau_f = \tau_0 \times \Phi_f$$

Where

τ_0 : Theoretical radiative lifetime in ns

Φ_f : Fluorescence quantum yield

Calculation of theoretical fluorescence lifetime of PP-PMI in CHL:

$$\tau_f = \tau_0 \text{ x } \Phi_f$$

τ_f = 3.88 ns X 0.07 = 0.27 ns

Table 4.5 illustrates the calculated theoretical fluorescence lifetime (τ_f) for the synthesized compounds in different solvents.

Table 4.5: Theoretical Fluorescence Lifetime (τ_f) of PP-PDI and PP-PMI in different solvents.

Compound	Solvent	Φ_f	τ_0 (ns)	τ_f (ns)
PP-PDI	CHL	0.11	1.24	0.14
PP-PMI	CHL	0.07	3.88	0.27

4.6 Calculation of Fluorescence Rate Constants (k_f)

PP-PDI and PP-PMI theoretical fluorescence rate constant are calculated with the given equation below:

$$k_f = \frac{1}{\tau_0}$$

Where

k_f : fluorescence rate constant in s^{-1}

τ_0 : theoretical radiative lifetime in s

PP-PMI Fluorescence Rate Constant at λ_{max} = 547 nm in CHL:

$k_f = \frac{1}{1.55 \text{ X } 10^{-8}} = 6.4\ X\ 10^7 s^{-1}$

The same equation was used to calculate the theoretical rate constants of all the synthesized PP-PDI and PP-PMI and the results are presented in Table 4.6.

Table 4.6: Theoretical fluorescence rate constant of compounds PP-PDI and PP-PMI

Compound	Solvent	$\lambda_{max\ (nm)}$	τ_0 (s)	K_f (s^{-1})
PP-PDI	CHL	550	1.24×10^{-8}	8.1×10^{7}
PP-PMI	CHL	547	3.88×10^{-8}	2.5×10^{7}
PP-PDI	DMF	549	1.72×10^{-8}	5.8×10^{7}
PP-PMI	DMF	544	1.53×10^{-8}	6.5×10^{7}
PP-PDI	MeOH	547	9.40×10^{-8}	1.1×10^{7}
PP-PMI	MeOH	517	3.72×10^{-9}	2.6×10^{8}

4.7 Calculations of Oscillator Strengths (f)

A dimensionless quantity of an electron transition is called Oscillator strength denoted as f. The equation below can be used to calculate oscillator strength.

$$f = 4.32 \times 10^{-9} X \Delta \bar{\nu}_{1/2} X \varepsilon_{max}$$

Where

f: oscillator strength

$\Delta\bar{\nu}_{1/2}$: half-width of assigned absorption in cm^{-1}

ε_{max}: maximum extinction coeeficient in $L.mol^{-1}.cm^{-1}$ at λ_{max}

PP-PMI Oscillator strength in CHL:

$f = 4.32 \times 10^{-9} \; X \; \Delta \bar{\nu}_{1/2} \; X \; \varepsilon_{max}$

$f = 4.32 \times 10^{-9} \times 31000 \times 870.02 = 0.12$

***f* = 0.12**

Oscillator strength of synthesized compounds of PP-PMI and PP-PDI are represented in Table 4.7

Table 4.7: Oscillator strengths of PP-PMI and PP-PDI in different solvents

Compound	**Solvent**	**λ_{max} (nm)**	**$\Delta\bar{\nu}_{1/2}$ (cm^{-1})**	**ε_{max} ($M^{-1}cm^{-1}$)**	***f***
PP-PDI	CHL	550	943.54	90000	0.36
PP-PMI	CHL	547	870.02	31000	0.12
PP-PDI	DMF	549	916.49	67000	0.27
PP-PMI	DMF	544	1126.07	60000	0.29
PP-PDI	MeOH	547	150.48	74000	0.04
PP-PMI	MeOH	517	1875.68	134000	1.09

4.8 Calculations of Singlet Energies (E_s)

The amount of energy needed by a chromophore to carry out an electronic transition from its ground state to an excited state is known as its singlet energy. Singlet energy can be calculated with the application of the following formula,

$$\mathbf{E_s} = \frac{\mathbf{2.86\ x\ 10^5}}{\boldsymbol{\lambda}_{\mathbf{max}}}$$

Where

E_s : Singlet energy in kcal mol^{-1}

λ_{max} : Maximum absorption wavelength in Å

Singlet energy of PP-PMI at λ_{max} = 547 nm:

$$E_s = \frac{2.86\ x\ 10^5}{\lambda_{max}} = \frac{2.86\ x\ 10^5}{5470} = 52.29 \text{ kcal mol}^{-1}$$

The singlet energies of PP-PDI and PP-PMI were calculated and reported as follows on Table 4.8

Table 4.8: Singlet energies of PP-PMI and PP-PDI in different solvents

Compound	Solvent	λ_{max} **(Å)**	E_s **(kcal mol^{-1}**
PP-PDI	CHL	550	52.00
PP-PMI	CHL	547	52.29
PP-PDI	DMF	549	52.09
PP-PMI	DMF	544	52.57
PP-PDI	MeOH	547	52.9
PP-PMI	MeOH	517	55.32

4.9 Calculations of Optical Band Gap Energies (E_g)

Highest Occupied Molecular Orbital and Lowest Unoccupied Molecular Orbital energy levels are significant parameters in solar cell applications specifically. Band gap energy gives important information as concerns HOMO and LUMO energy levels. It is calculated through the application of the following equation.

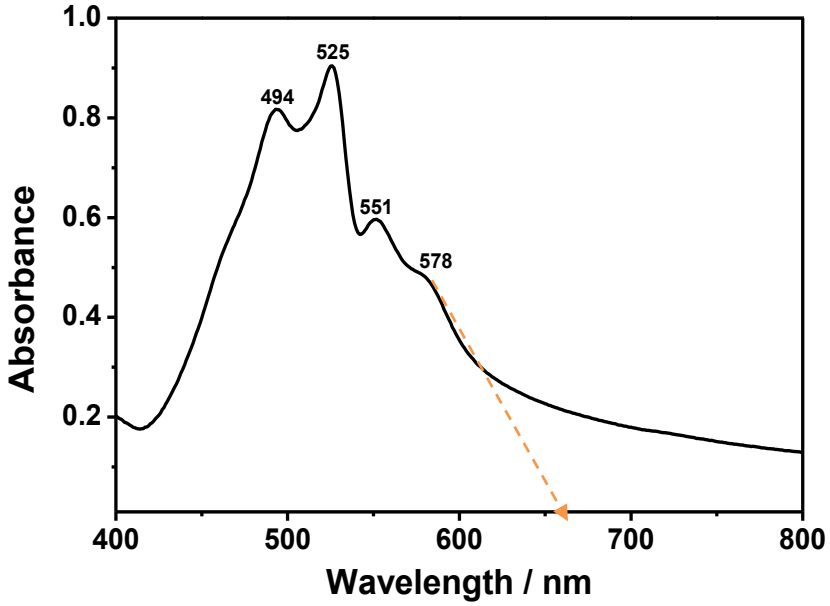

Figure 4.3: Absorption Spectrum of PP-PMI and Cut-off wavelength

$$E_g = \frac{1240\ eV\ nm}{\lambda}$$

Where

E_g : Band gap energy measured in eV

λ : cut-off wavelength of the absorption band gap in nm

Band gap energy for PP-PMI in CHL:

As illustrated by Figure 4.3, the cut-off wavelength of the absorption band is gotten via extrapolation of the maximum absorption band to the zero absorbance.

$$E_g = \frac{1240\ eV}{\lambda} = \frac{1240\ eV}{651.02} = \mathbf{1.90\ eV}$$

The band gap energies of all synthesized compounds of PP-PDI and PP-PMI were calculated and presented on Table 4.9.

Table 4.9: Band Gap energies of PP-PMI and PP-PDI

Compound	**Solvent**	**λ_{max} (nm)**	**Cut-off (nm)**	**λ**	**E_g (eV)**
PP-PDI	CHL	550	665.75		1.86
PP-PMI	CHL	547	651.02		1.90
PP-PDI	DMF	549	650.05		1.91
PP-PMI	DMF	544	634.19		1.96
PP-PDI	MeOH	547	652.08		1.90
PP-PMI	MeOH	517	536.82		2.31

4.10 Thin Layer Chromatography (TLC) of PP-PDI and PP-PMI

Thin layer chromatography (TLC) is a technique used in the analysis of mixtures via the separation of the constituting compounds of the mixture. TLC is used to determine the amount or number of components in a mixture, to identify a compound, and to purify a compound. Looking at the appearance of the product of the disappearance of the reactant serves as a monitoring aid to the progress of reactions.

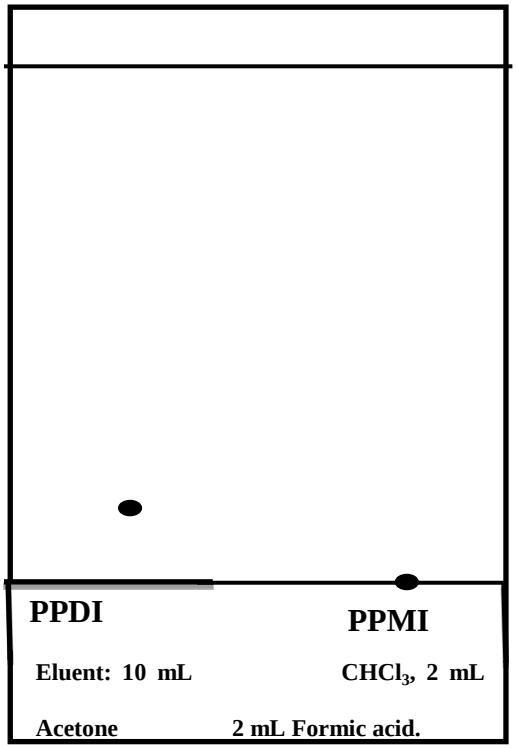

Figure 4.20: TLC of PPDI and PP

Figure 4.20 shows the thin layer chromatography (TLC) analysis for PPDI and PPMI, CHL, acetone and formic acid mixture (10:2:2) is used as eluent. The R_f value of PPDI is calculated to be 2.41%. On the other hand, since PPMI is more polar than PPDI it never moved or ran as compared to the less polar PPDI.

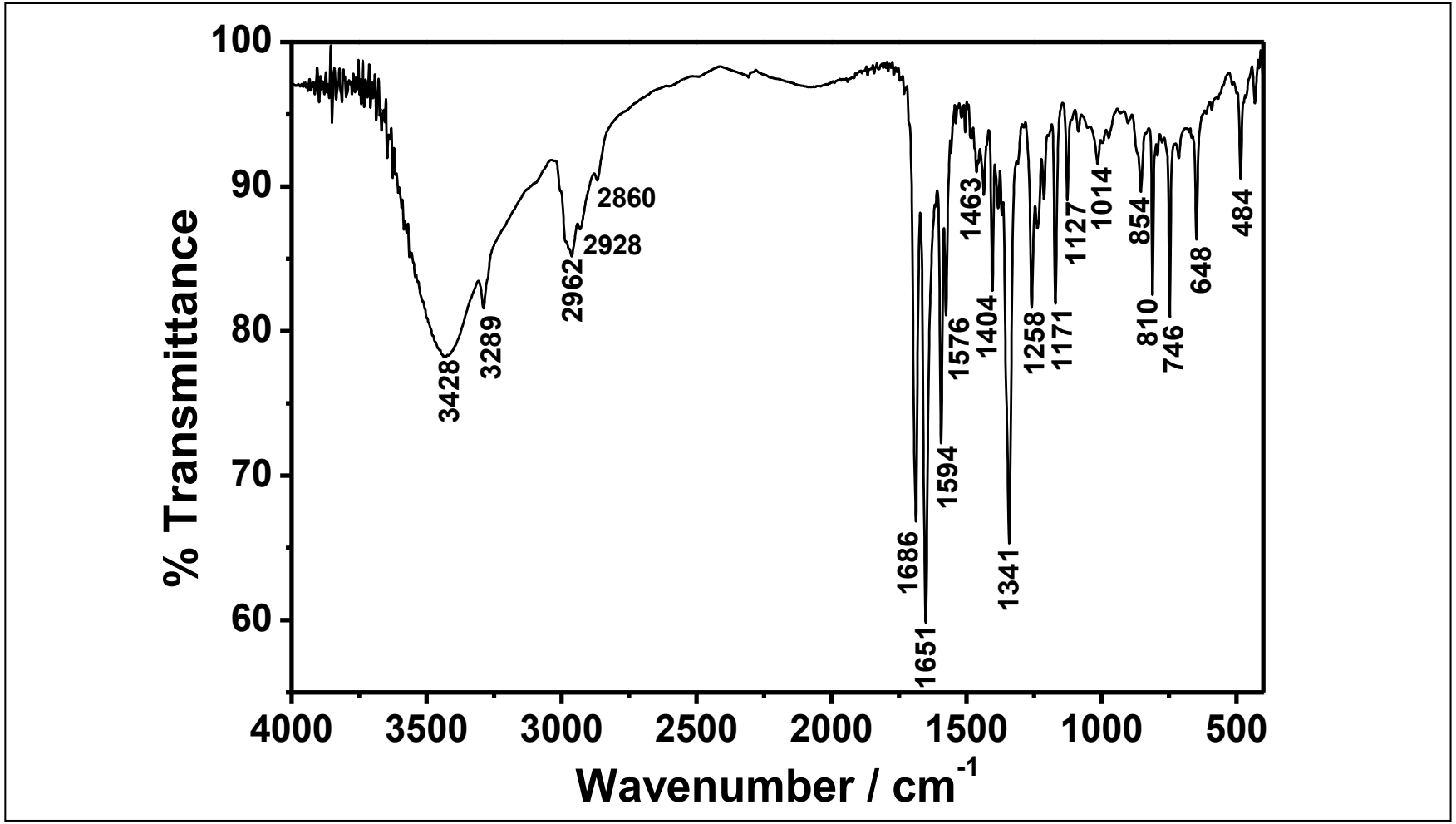

Figure 4.4: FTIR spectrum of PP-PDI

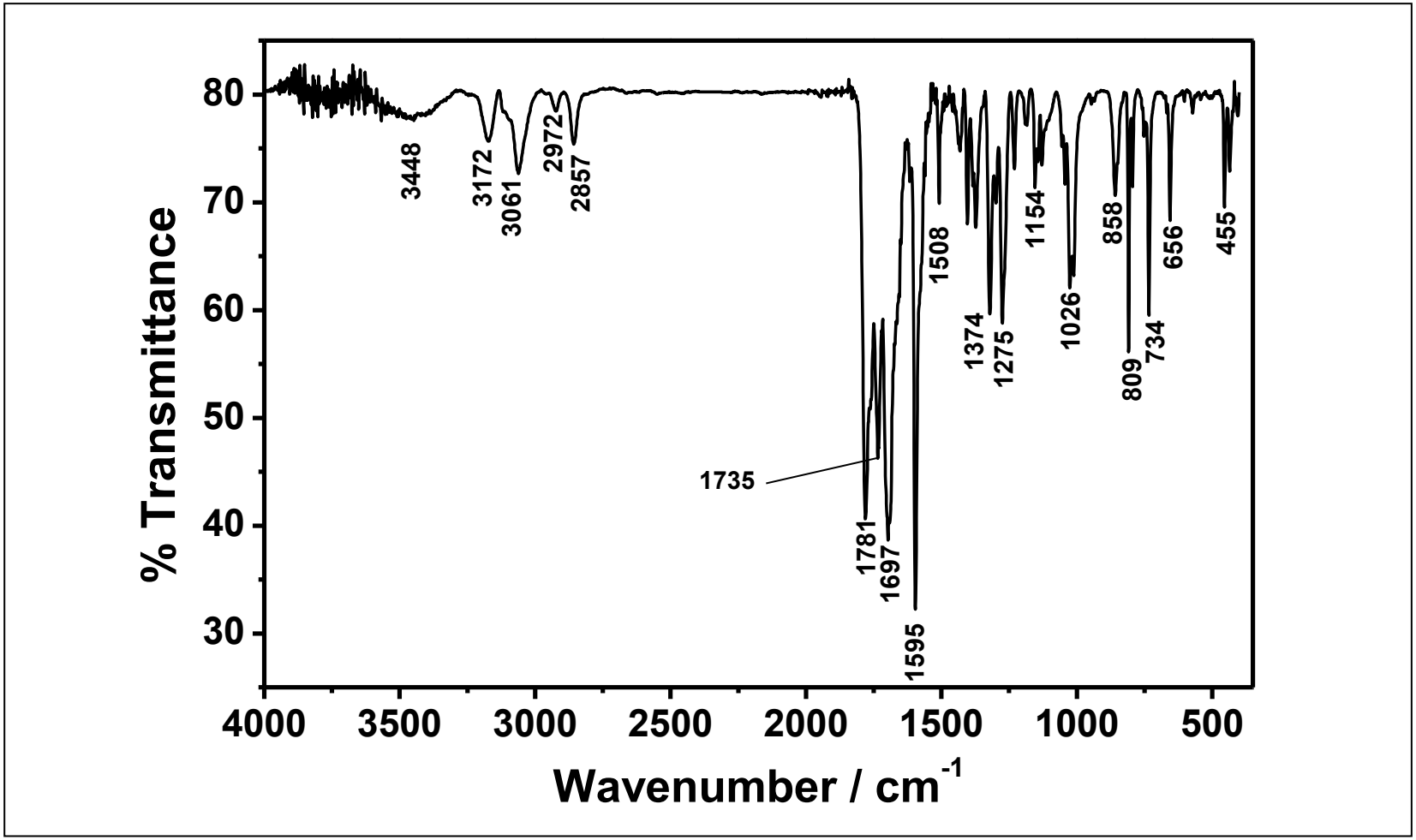

Figure 4.5 FTIR spectrum of PP-PMI

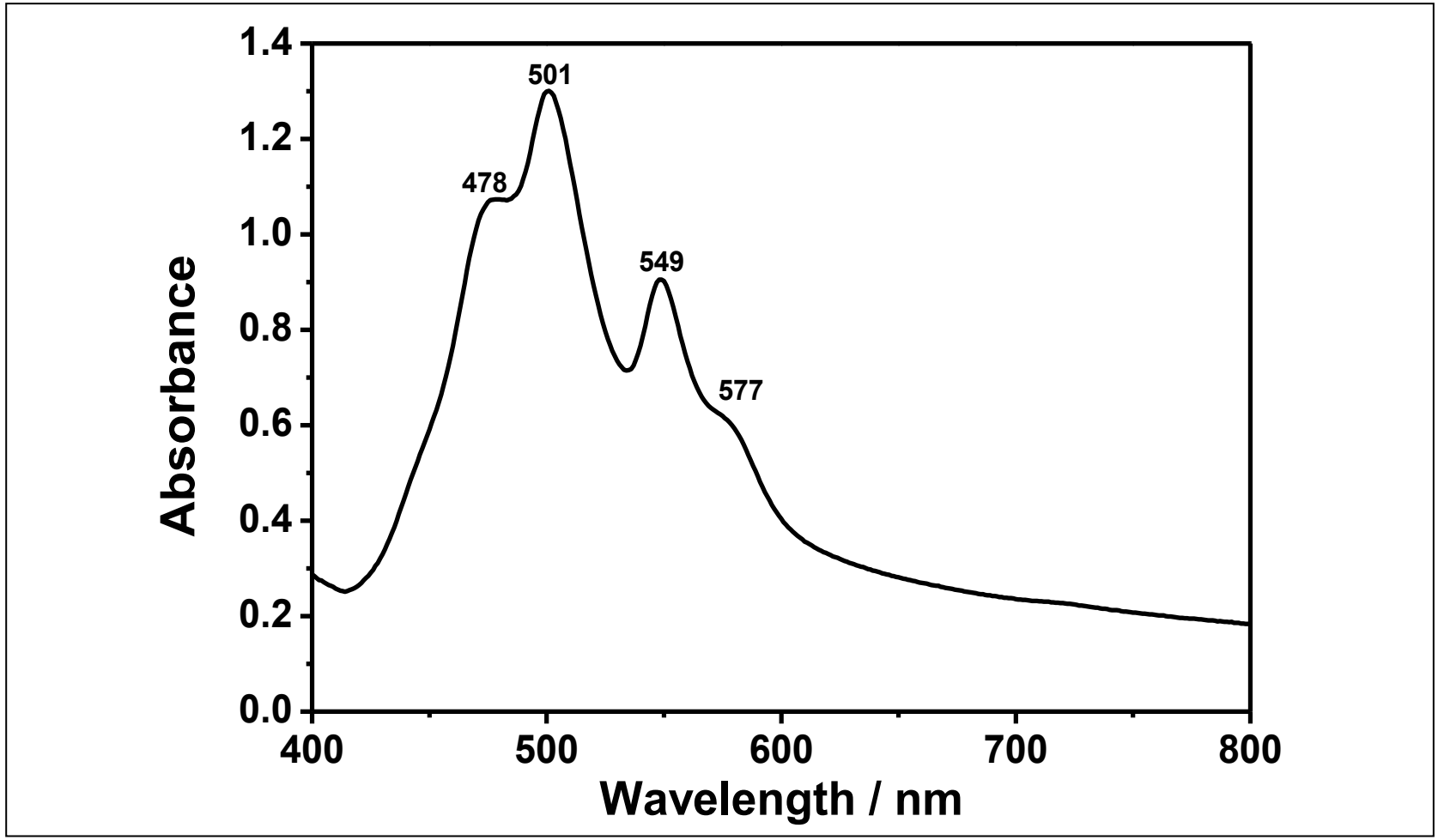

Figure 4.6: Absorbance spectrum of PP-PDI in DMF

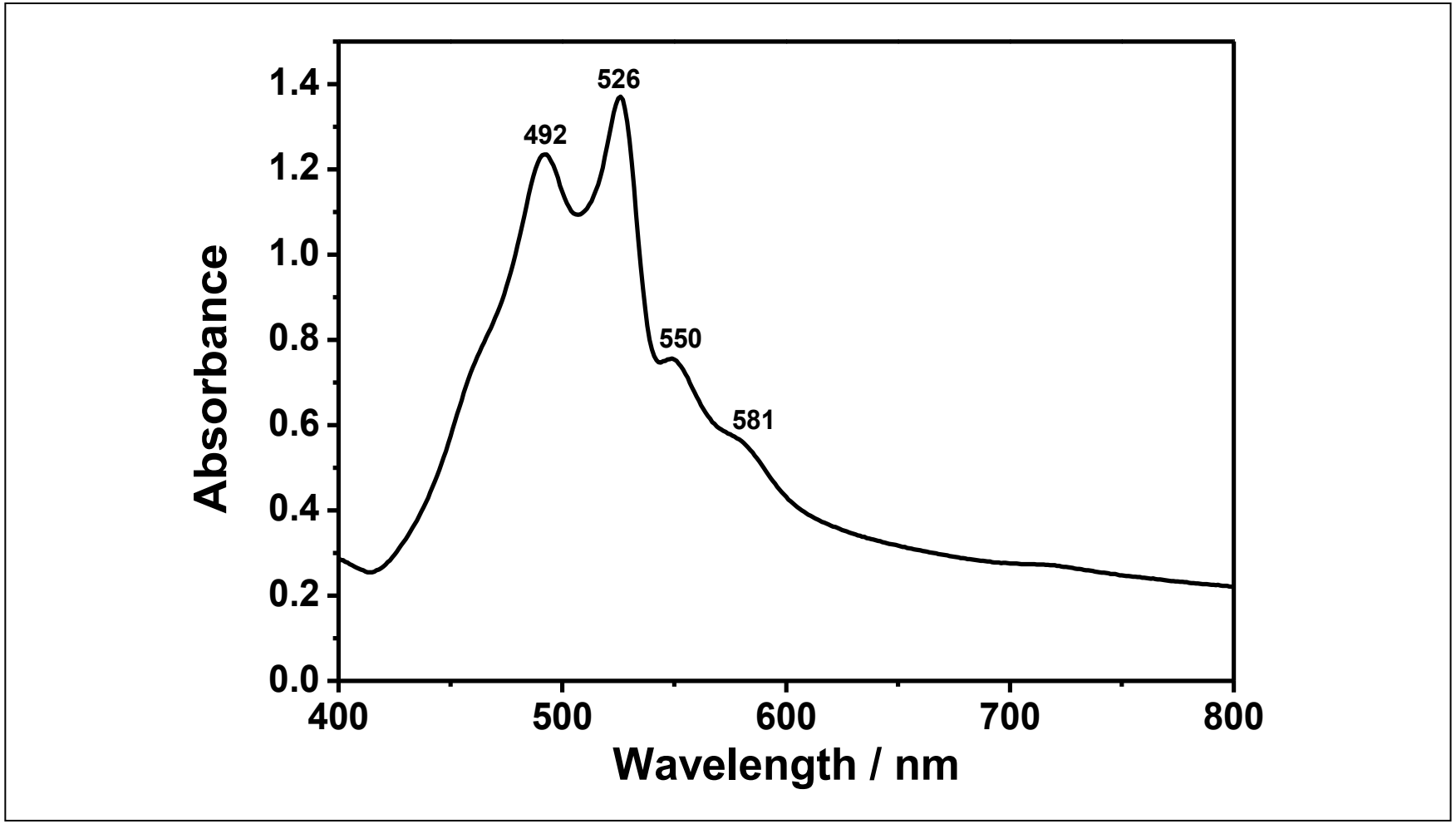

Figure 4.7: Absorbance spectrum of PP-PDI in CHL

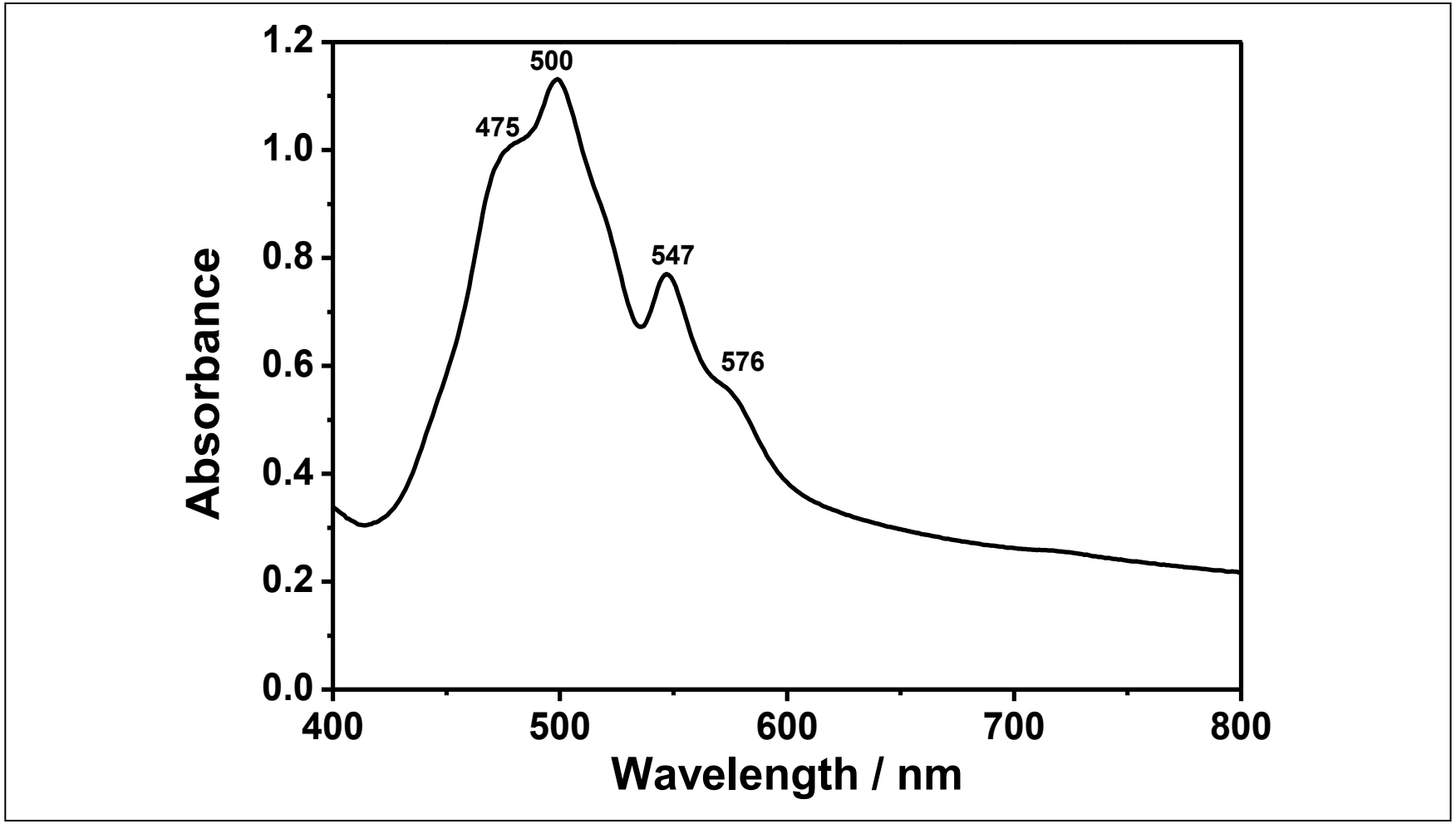

Figure 4.8: Absorbance spectrum of PP-PDI in MeOH

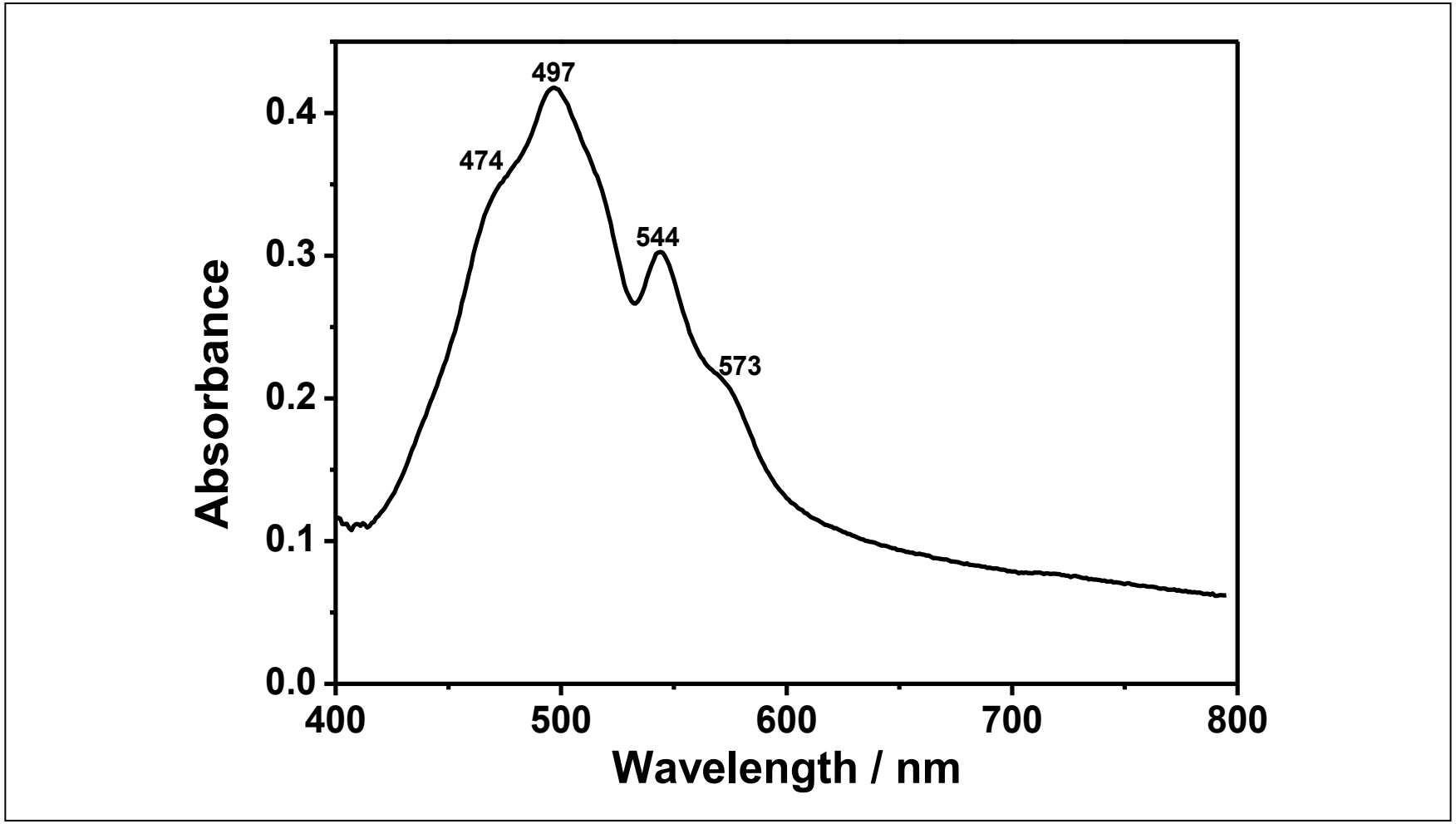

Figure 4.9: Absorbance spectrum of PP-PMI in DMF

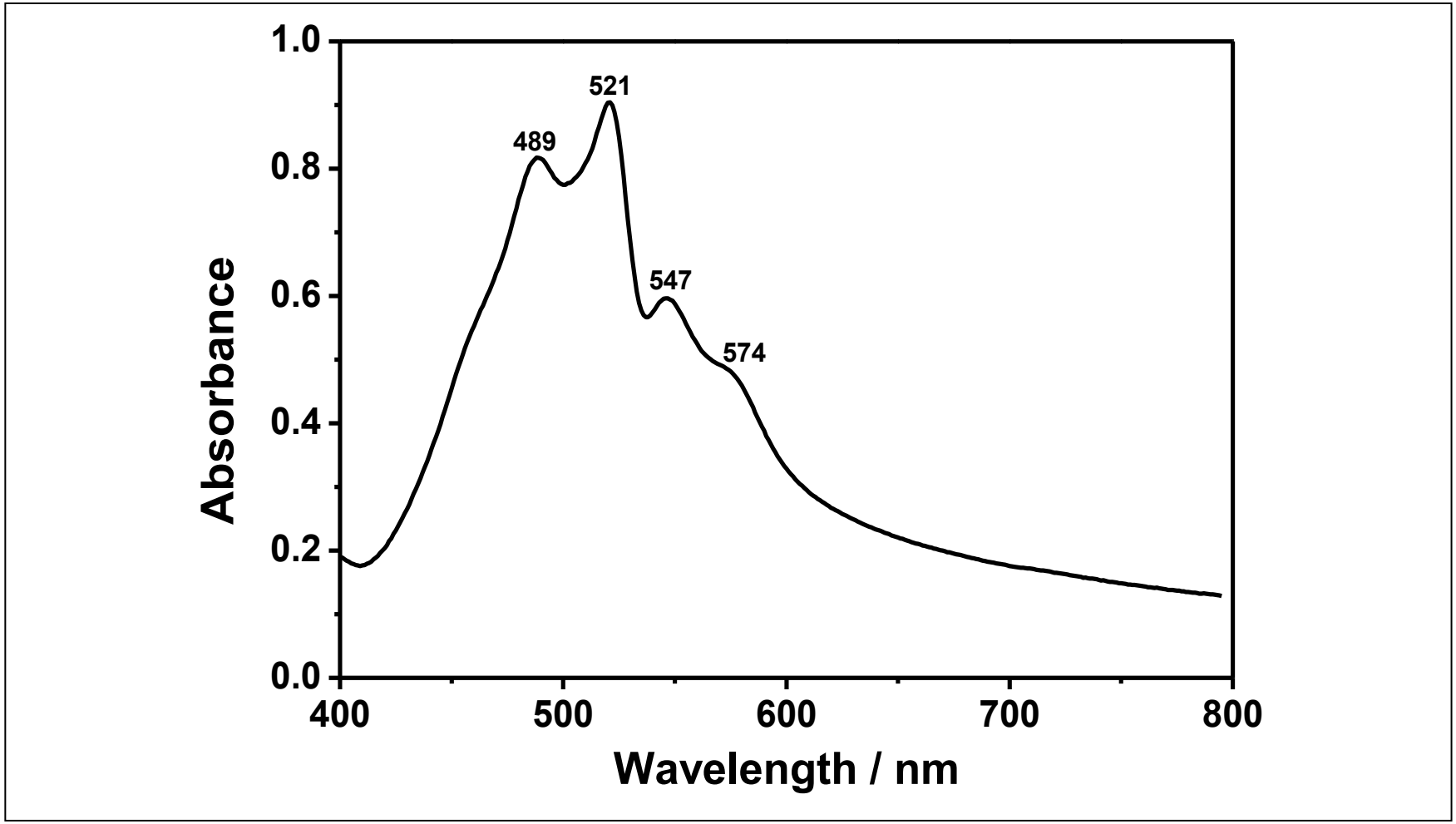

Figure 4.10: Absorbance spectrum of PP-PMI in CHL

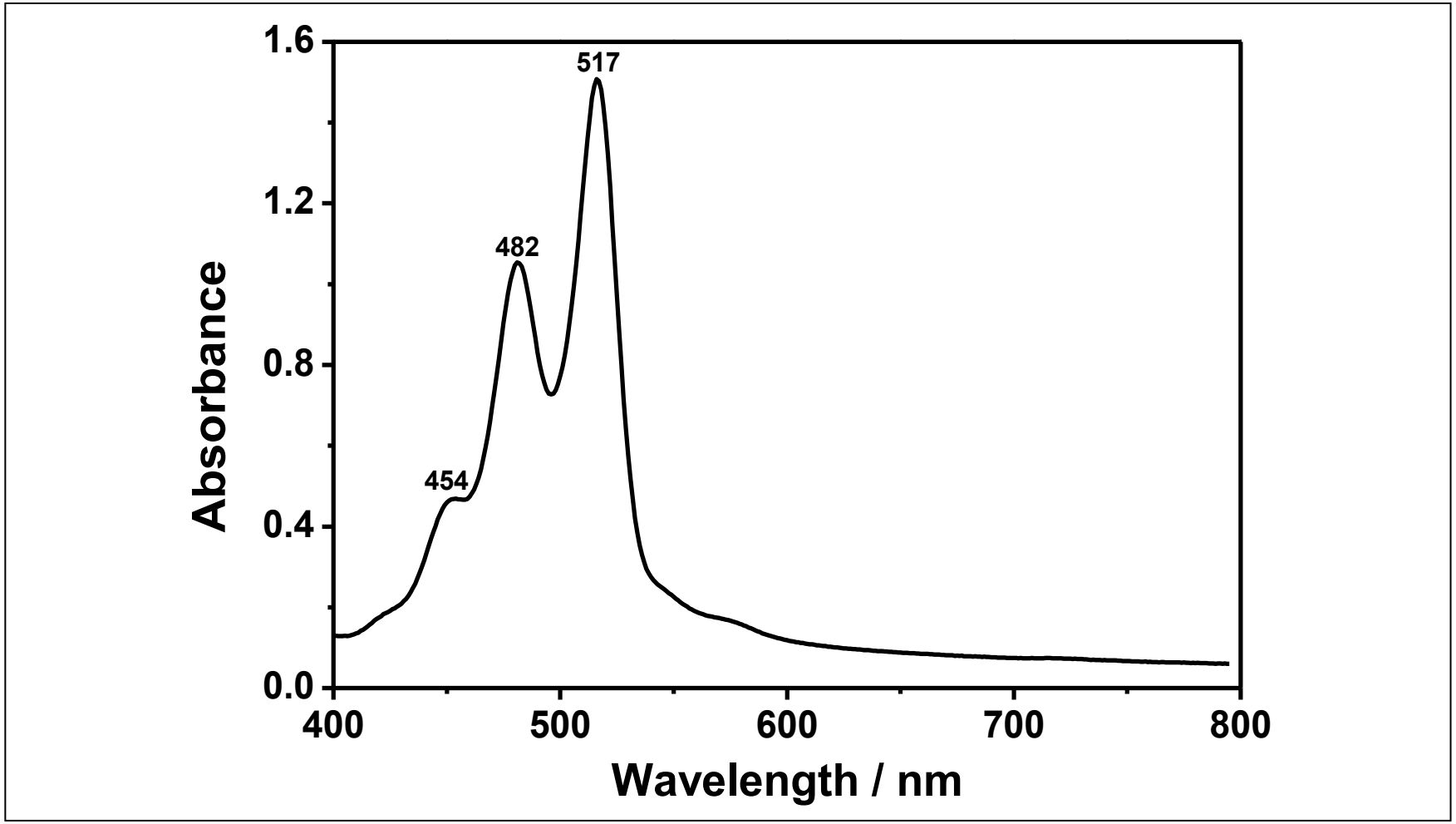

Figure 4.11: Absorbance spectrum of PP-PMI in MeOH

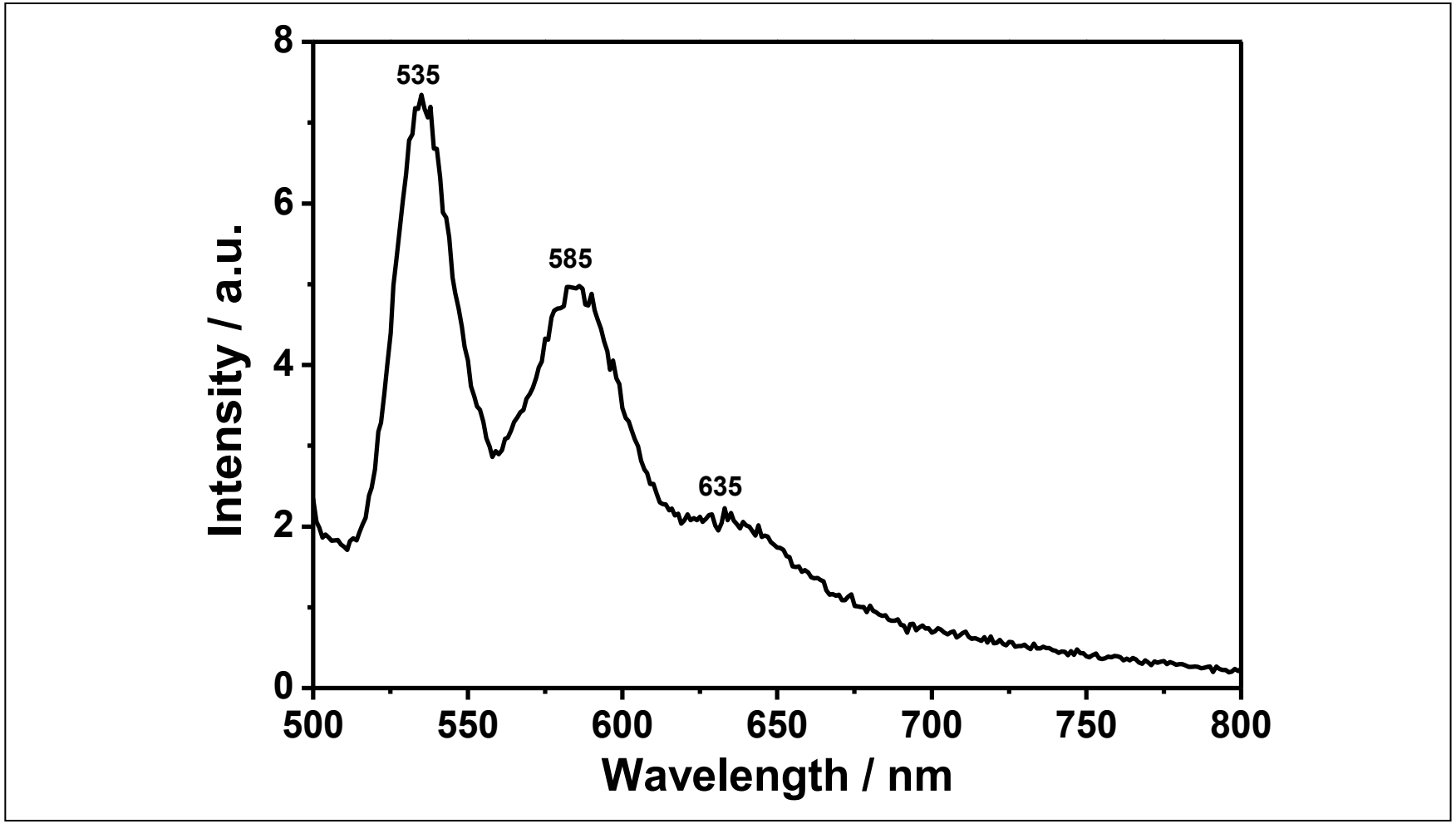

Figure 4.12: Emission spectrum of PP-PDI in DMF

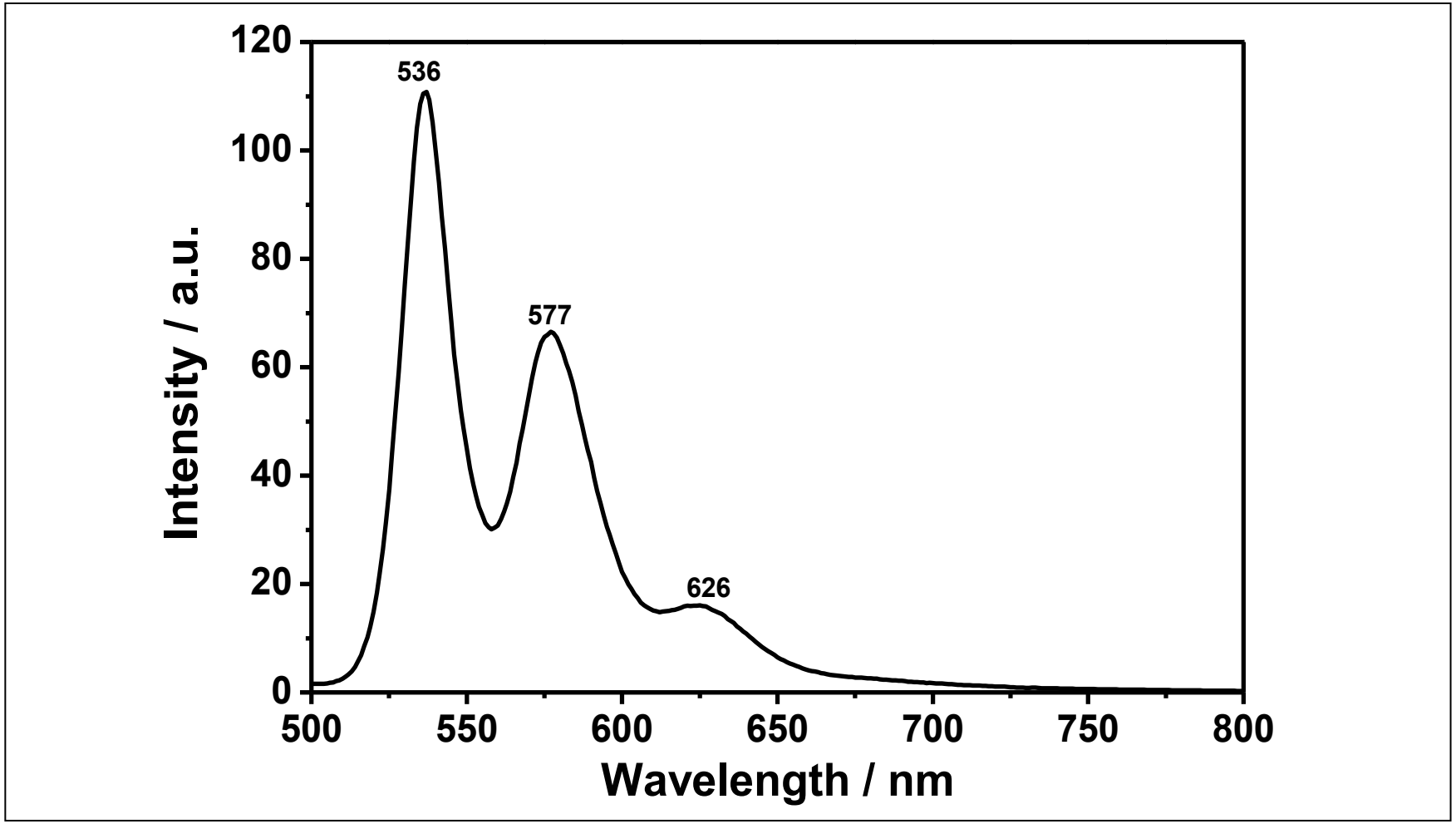

Figure 4.13: Emission spectrum of PP-PDI in CHL

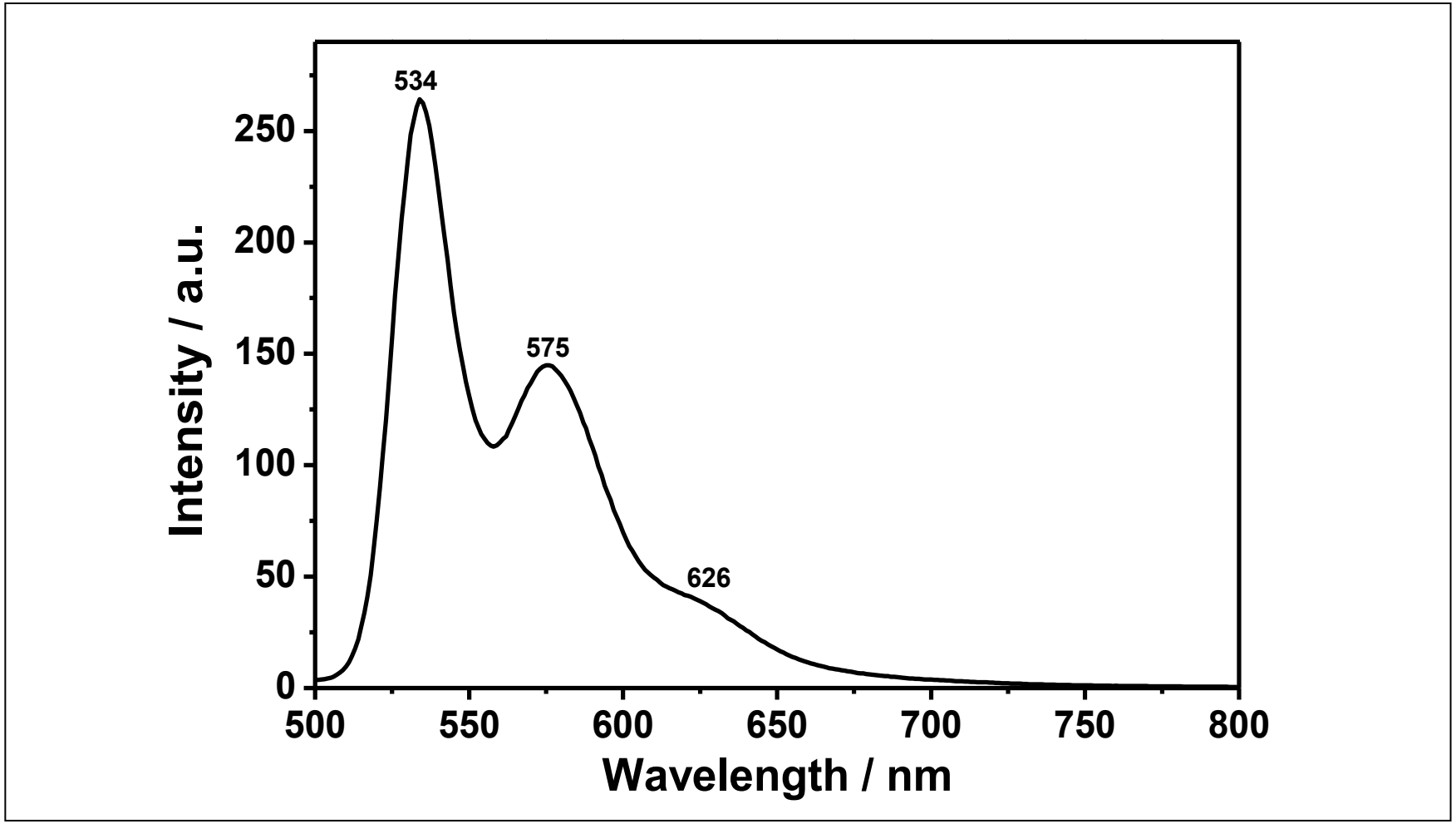

Figure 4.14: Emission spectrum of PP-PDI in MeOH

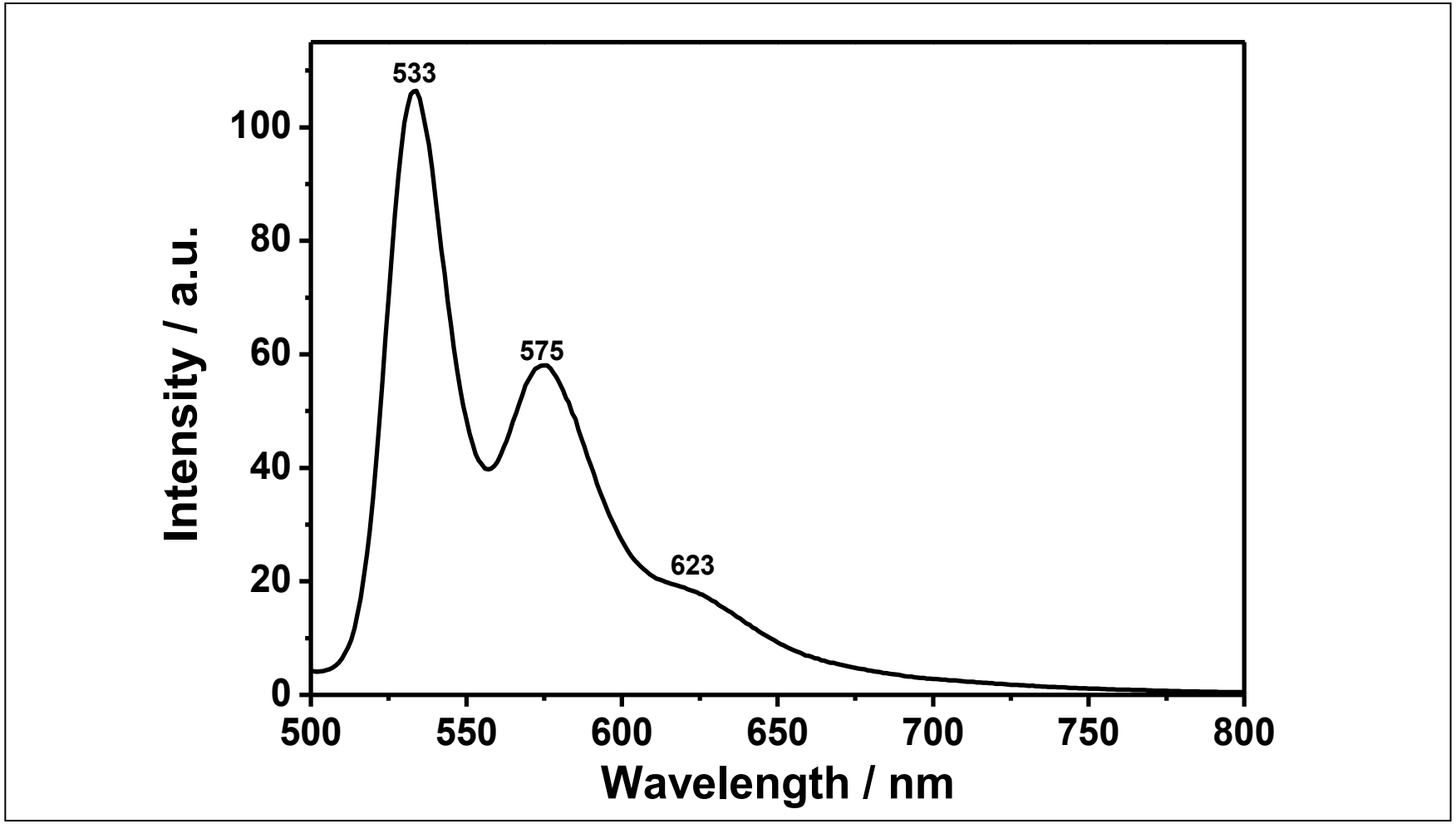

Figure 4.15: Emission spectrum of PP-PMI in DMF

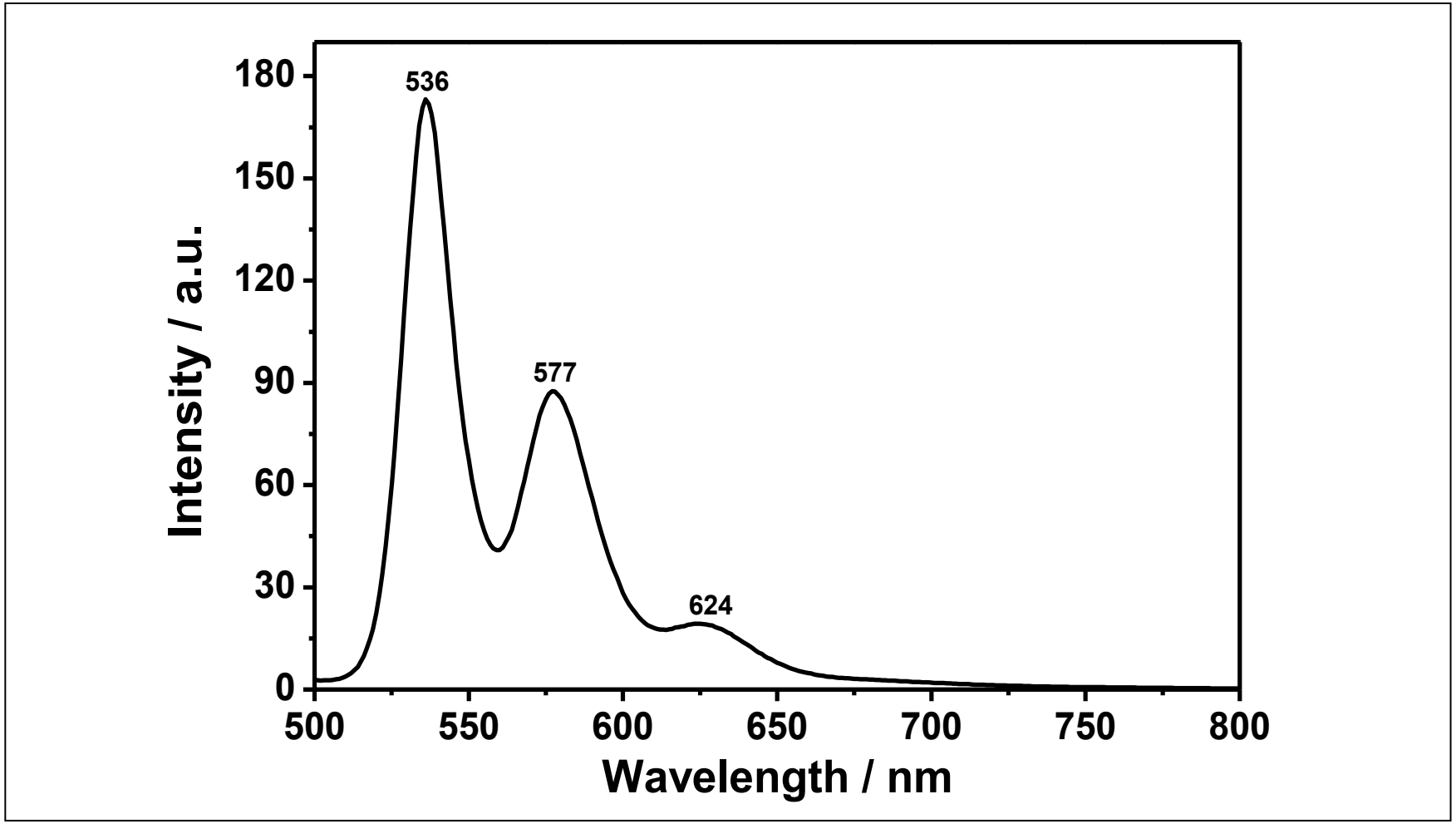

Figure 4.16: Emission spectrum of PP-PMI in CHL

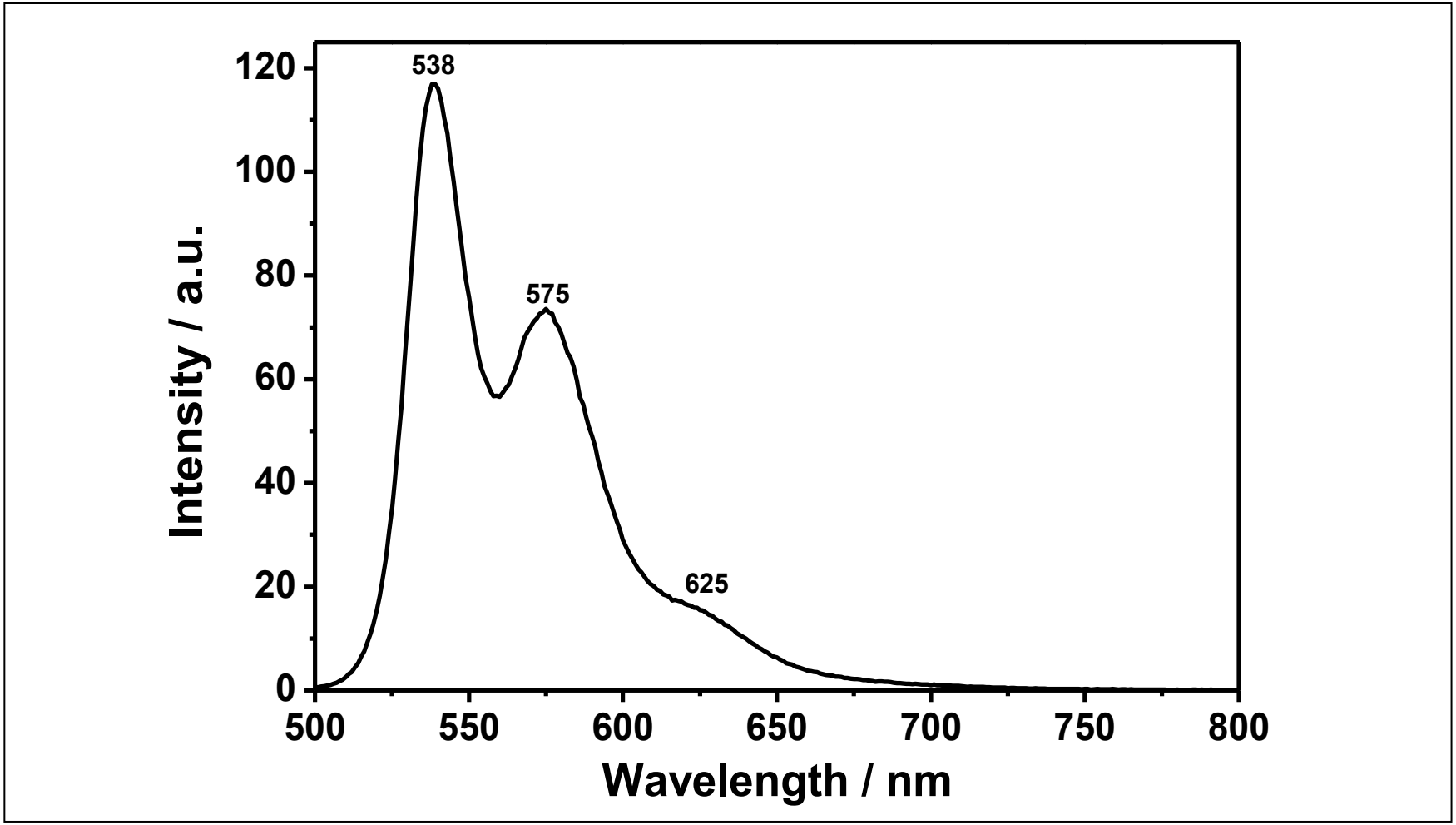

Figure 4.17: Emission spectrum of PP-PMI in MeOH

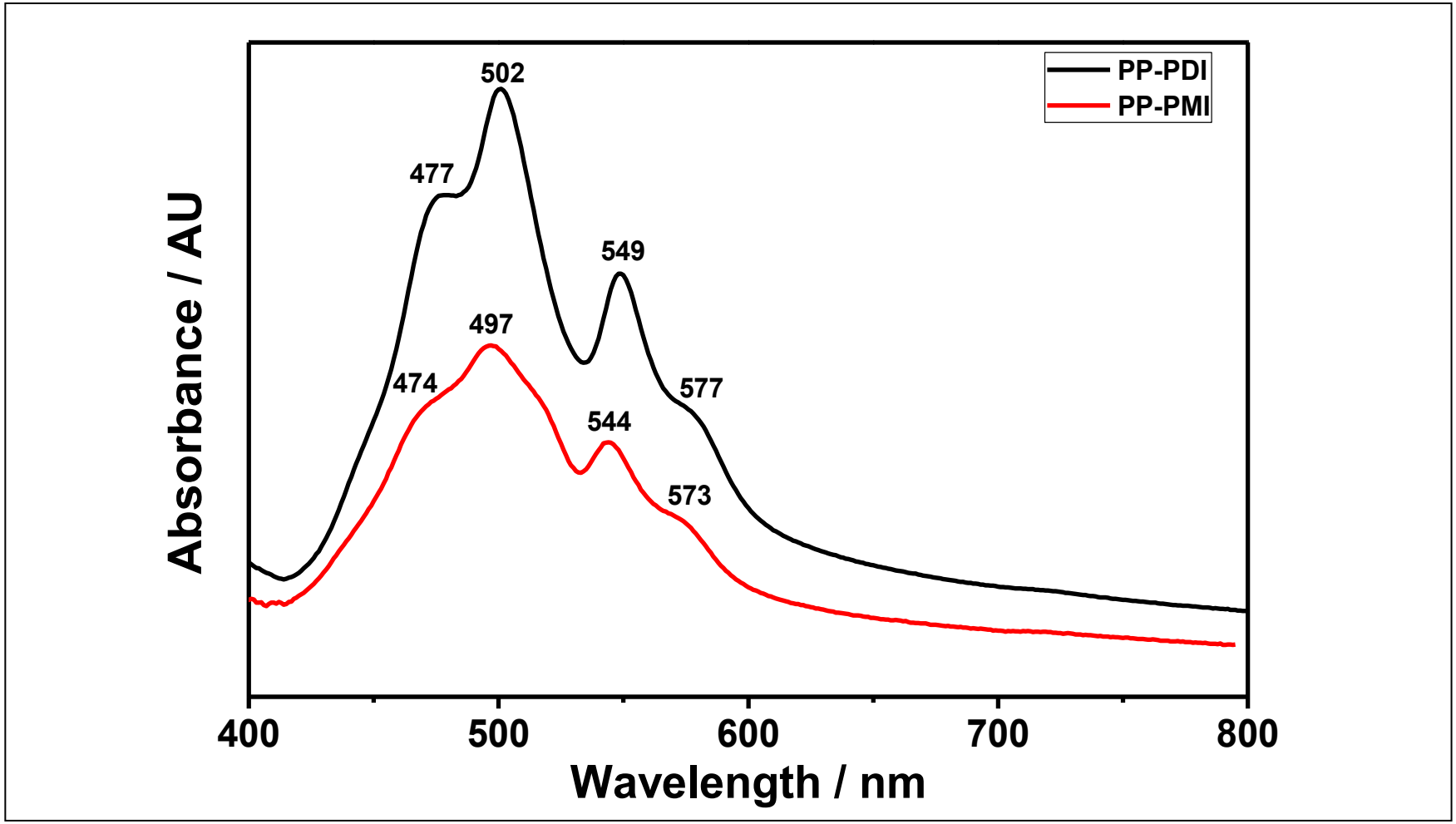

Figure 4.18: Absorption spectra of PP-PDI and PP-PMI in DMF

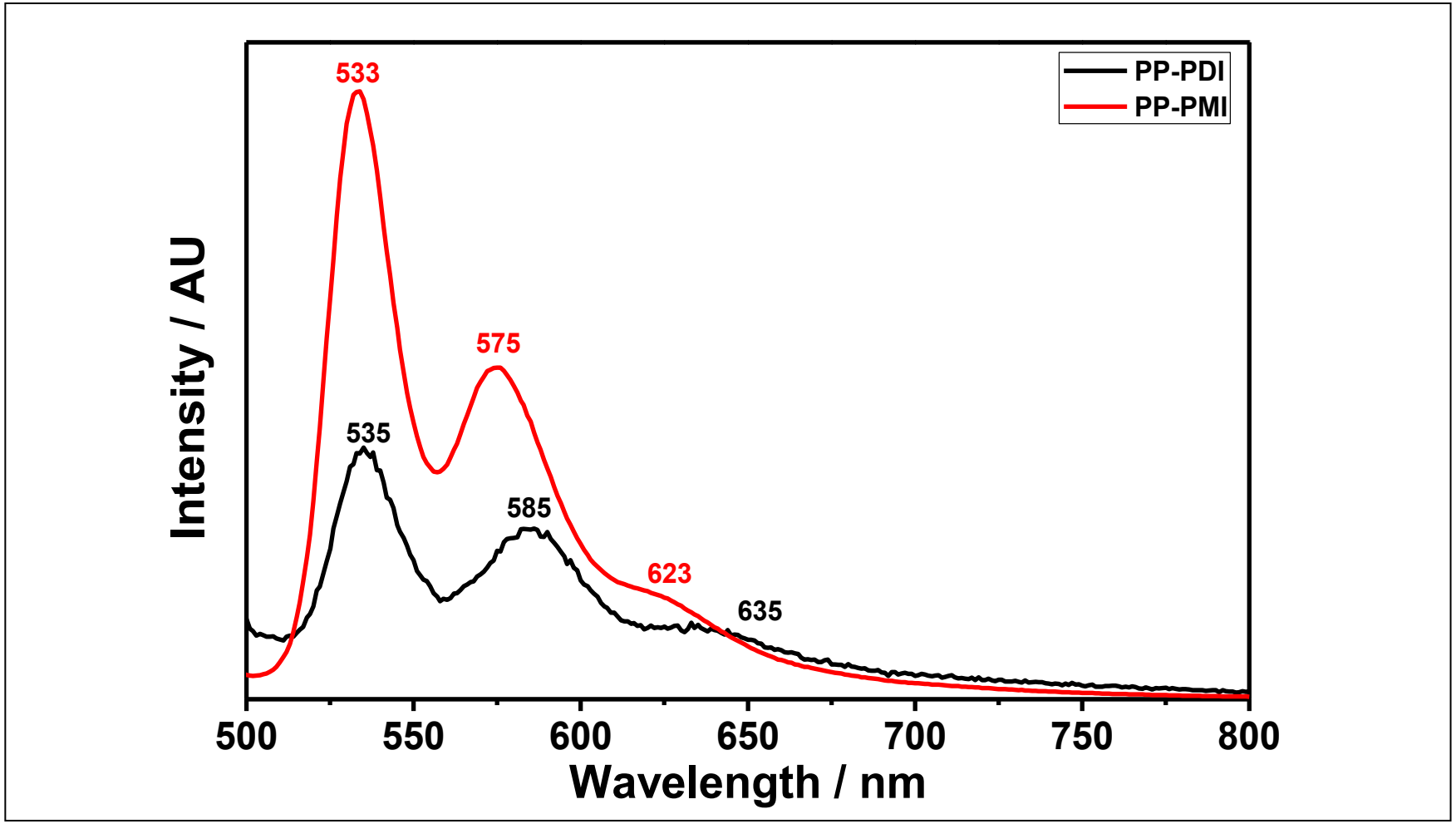

Figure 4.19: Emission spectra of PP-PDI and PP-PMI in DMF

Chapter 5

RESULTS AND DISCUSSION

5.1 Synthesis and solubility of Perylene Dyes

5.1.1 Synthesis of Perylene Dyes

Perylene dyes due to their outstanding properties are well known dyes and according to their electron-accepting properties they are used in the solar cell applications as n-type materials. In this Thesis, a perylene diimide, PP-PDI and a perylene monoimide (PP-PMI) were successfully synthesized. PP-PDI was successfully synthesized from PDA by condensation reaction in a single step. Later PP-PMI was synthesized from the previously obtained PP-PDI by reacting it with KOH. Both of the products were obtained with high yields. They have synthesized according to the procedures and reactions were followed up by TLC and FTIR spectra. At the end of the reaction, the photophysical properties of PPDI and PPMI are discussed in this work.

5.1.2 Solubility of Perylene Dyes *1.1.1.1*

All the synthesized perylene dyes showed good solubility in basic organic solvents. PP-PDI has an excellent solubility in dipolar aprotic solvent, even at room temperature. DMF was partially soluble in CHL and MeOH. PP-PMI was partially soluble in both aprotic and protic solvents, i.e. DMF, CHL and MeOH. Table 5.1 shows all the solubility properties of both PPDI and PPMI.

Table 5.1: Solubility of PP-PDI and PP-PMI

	Solubility/color	
Solvent	**PP-PDI**	**PP-PMI**
DMF	(+ +)/ Pink-Red	(– +)*/Pink-Red
CHL	(– +)*/ Pink-Red	(– +)/Pink-Red
MeOH	(– +)*/Pink-Red	(– +)/Pink-Red

(+/+): Soluble at RT, (+/-): Partially soluble at RT, (*): Solubility increases on heating.

5.2 Structural Characterization

5.2.1 FTIR Spectra Analysis

Confirmation of functional groups present in the compounds (PP-PDI and PP-PMI) was characterized basically by FTIR spectra. The spectra showed all the functional groups found in both the structures. The analysis of all the FTIR spectra of both PPDI and PPMI are given below.

Figure 4.3 shows N-H stretching at 3428 and 3289 cm^{-1}, C-H aromatic stretching at 3062 cm^{-1}, C-H aliphatic stretching at 2962 cm^{-1}, 2928 cm^{-1} and 2860 cm^{-1}, C=O imide stretching at 1651 cm^{-1} and 1686 cm^{-1}, conjugated C=C stretching at 1594 cm^{-1}, and 1576 cm^{-1}, C-N stretching at 1341 cm^{-1}, C-H aromatic bending at 810 cm^{-1}, and 746 cm^{-1} that confirms the structure of a PPDI.

Figure 4.4 shows N-H stretching at 3274 cm^{-1}, aromatic C-H at 3062 cm^{-1}, anhydride C=O stretching at 1762 cm^{-1}, 1734 cm^{-1}, imide C=O stretchings at 1700 cm^{-1} and 1656 cm^{-1}, C=C conjugated stretching at 1598 cm^{-1}, C-N stretching at 1413 cm^{-1}, anhydride C-O stretching at 1060 cm^{-1}, C-H aromatic bending at 883 cm^{-1}, 811 cm^{-1}, and 701 cm^{-1} that confirms the structure of a PPMI.

5.2.2 UV-vis spectra interpretation

The UV-vis absorption spectra of both PDI and PMI were studied in different solvents. The absorption spectra of each compound were interpreted below.

Absorption spectra of PP-PDI are illustrated in Figures 4.5 – 4.8 in various solvents.

Figure 4.5 shows the PP-PDI absorption spectrum in diprotic apolar solvent, DMF. There are four peaks at 478, 501, 549 and 577 nm. The first three are characteristic peaks due to the π-π interactions of the conjugated perylene structure. The fourth peak at 577 nm is attributed to the aggregation. The aggregate formation is also supported from the shape of three characteristic peaks, they are not resolved. Table 4.2 shows that in DMF, PPPDI has high molar extinction coefficient (ε_{max} = 31000$M^{-1}cm^{-1}$) which indicates that PDI has strong absorptivity character in the visible region.

The absorption spectrum of PPPDI in nonpolar solvent, CHL, is shown in Figure 4.6. In this spectrum, again three characteristics absorption peaks at 492, 526, and 550 nm, respectively were observed due to π-π interactions. The fourth peak at 581 nm is attributed to the aggregation. The O→O transition peak both DMF and CHL are similar. On the other hand, O→1 transition peak in CHL has 25 nm bathochromic shifts. The peaks are more resolved in non-polar solvent than aprotic solvent.

Figure 4.7 shows the absorption spectrum of PP-PDI in polar protic solvent, MeOH. There are four absorption peaks were observed as well, similar to dipolar protic solvent, DMF.

The absorption spectrum of PP-PDI in polar solvent, MeOH is shown in Figure 4.8. PP-PDI has three characteristic absorption peaks at 475, 500, and 547 nm respectively like in dipolar aprotic solvent, DMF. The aggregation peak is observed again at 576 nm.

The absorption spectrum of PP-PMI in dipolar aprotic solvent, DMF, is shown in Figure 4.9. The absorption peaks of PP-PMI are very similar to the absorption peaks of PP-PDI (Figure 4.18). There is 5nm hypsochromic shift observed in the spectrum of PPMI by comparing PPDI. The aggregation is higher in PPMI since the peaks of PPDI are more resolved than PPMI.

Figure 4.10 shows the absorption spectrum of PP-PMI in nonpolar solvent, CHL. There are four absorption peaks observed. The peaks are at 489, 521, 547 and 574 nm respectively. The first three peaks are attributed to the π-π interactions of conjugated perylene structure. The fourth peak represents the aggregate formation. The molar extinction coefficients of PP-PMI in CHL (ε_{max} = 60000 $M^{-1}cm^{-1}$) indicates the strong absorption properties in the visible region. Like in dipolar aprotic solvents 5nm hypsochromic shift also observed. In non-polar solvents, Figure 4. 17 show the absorption spectrum of PP-PMI in polar protic solvent, MeOH.

Three well resolved absorption peaks were observed at 454, 482, and 517 nm, respectively. There is a small shoulder at higher at higher wavelength around 550-600 nm region. The observed absorption peaks that is attributed to π-π interactions of conjugated perylene structure. This well resolved absorption peaks indicates that almost no aggregation observed in MeOH. A hypsochromic shift (5nm) also observed in polar protic solvent.

5.2.3 Emission Spectra Interpretation

Figure 4.12 DMF-MeOH shows the emission spectra of PP-PDI in different solvents. All the emission spectra show three characteristic emission peaks represent the

O→O, O→1, O→2 transitions of perylene chromophore.

Figure 4.12, the three characteristic emission peaks at 535, 585 and 635 nm respectively, observed in dipolar aprotic solvent, DMF.

The emission spectra of PP-PDI shows (Figure 4.13) three characteristic emission peaks at 536, 577 and 626 nm respectively in nonpolar solvent, CHL.

Figure 4.14 shows the emission spectrum of PP-PDI. Three characteristic emission peaks observed at 534, 575 and 626 nm respectively in polar protic solvent, MeOH.

The absorption and emission spectra of PP-PDI in all the studied solvents were not mirror images of each other. On the other hand, the fourth peak that found in the absorption spectra has no significant effect on the emission spectra of the PP-PDI.

Figure 4.15 shows the emission spectrum of PP-PMI in dipolar aprotic solvent, DMF. Three characteristic emission peaks observed at around 533, 575 and 623 nm respectively which represents the O→O, O→1, O→2 transitions of perylene chromophore. On the other hand, the fourth peak found in absorption spectrum which represents the aggregation has no significant effect on the emission spectra of PP-PMI in DMF.

Figure 4.16 show the emission spectrum of PP-PMI in nonpolar solvents, CHL. Similarly, three characteristic emission peaks were observed at 536, 577 and 624 nm respectively.

Figure 4.17 shows the emission spectrum of PP-PMI in polar protic solvent, MeOH. Three characteristic emission peaks were observed at 538, 575, and 625 nm, respectively.

The absorption and emission spectra are mirror images of each other. There is no aggregation in the perylene monoimide in polar protic solvent, MeOH.

Chapter 6

CONCLUSION

In this thesis, a novel perylene monoimide N-(3,3,5,5-tetramethyl-4-piperidinyl)-3,4,9,10-perylenetetracarboxylic-3,4-anhydride-9,10-imide (PPMI) was successfully synthesized. In order to synthesized the designed perylene monoimide, as first step, perylene diimide, N,N'-Bis (3,3,5,5-tetramethyl 1-4-piperidinyl)-3,4,9,10-perylenebis-(dicarboximide) (PPDI) was synthesized. Both of the synthesized perylene derivatives were characterized by FT-IR spectra.

The optical properties of both PP-PDI and PP-PMI were studied by absorption and emission spectroscopy at different solvents.

The solubility of PP-PMI was decreased with respect to the PP-PDI as expected in common organic solvents [66].

The absorption spectra of both PP-PDI and PP-PMI in dipolar aprotic, nonpolar and polar protic solvents show three characteristic absorption peaks and a fourth peak which represents the aggregate formation. The emission spectra of both PP-PDI and PP-PMI in the studied solvents (dipolar aprotic, nonpolar and polar protic) shows three characteristic emission peaks.

The absorption and emission spectra of all are not mirror images of each other except PP-PMI in polar protic solvent, MeOH. Ineterestingly, the fourth peaks that

observed in the absorption spectra have no effect on the emission properties of both PP-PDI and PP-PMI.

According to the properties of PP-PMI, it has high potential in solar cell applications.

REFERENCES

[1] Flors, C., Oesterling, I., Schitzler, T., Fron, E., Schweitzer, G., Sliwa, M., Herrmann, A., Auweraer, M.V.D., Schryver, F.C.D., Müllen, K., & Hofkens, J. (2007) Energy And Electron Transfer In Ethynylene Bridged Perylene Diimide Multichromophores. *J. Phys. Chem.* 111: 4861-4870.

[2] Alvino, A., Franceschin, M., Cefaro, C., Borioni, S., Ortaggi, G., & Bianco, A. (2007) Synthesis And Spectroscopic Properties Of Highly Water-Soluble Perylene Derivatives. *Tetrahedron.* 63:7858-7865.

[3] Bagui, M., Dutta, T., Zhong, H., Li, S., Chakraborty, S., Keightley, A., & Peng, Z. (2012) Synthesis And Optical Properties Of Perylene Diimide Derivatives With Triphenylene-Based Dendrons Linked At The Bay Positions Through A Conjugated Ethynyl Linkage. *Tetrahedron.* 68:2806-2818.

[4] Bo, L., MinMin, S., Ligong, Y., HongZheng, C., & Mang, W. (2008) Synthesis Of A Novel Perylene Diimide Derivative And Its Charge Transfer Interaction With C_{60} .*Sci. China Ser B-Chem.* 51: 152-157.

[5] Bodapati, J.B., & Icil, H. (2008) Highly Soluble Perylene Diimide And Oligomeric Diimide Dyes Combining Perylene And Hexa (Ethylene Glycol) Units: Synthesis, Characterization, Optical And Electrochemical Properties. *DYES PIGMENTS*. 79: 224-235.

[6] Boni, L.D, Constantino, C.J.L., Misoguti, L., Aroca, R.F., Zilio, S.C., & Mendonça, C.R. (2003) Two-Photon Absorption In Perylene Derivatives. *Chem. Phys. Lett.* 371:744-749.

[7] Fortage, J., Séverac, M., Houarner-Rassin, C., Pellegrin, Y., Blart, E., & Odobel, F. (2008) Synthesis Of New Perylene Imide Dyes And Their Photovoltaic Performances In Nanocrystalline TiO_2 Dye-Sensitized Solar Cells. *J. Photochem. Photobiol.*, A. 197:156-169.

[8] Perrin, L., & Hudhomme, P. (2011) Synthesis, Electrochemical And Optical Absorption Properties Of New Perylene-3,4:9,10-bis(Dicarboximide) And Perylene-3,4:9,10-bis(Benzimidazole) Derivatives. *Eur. J. Org. Chem*. 2011: 5427-5440.

[9] Singh, Th.B., Erten, S., Günes, S., Zafer, C., Turkmen, G., Kuban, B., Teoman, Y., Sariciftci, N.S. & Icil, S. (2006) Soluble Derivatives Of Perylene And Naphthalene Diimide For n-Channel Organic Field-Effect Transitors. *Org. Electron*. 7:480-489.

[10] Salvan, G., Silaghi, S., Friedrich, M., Himcinschi, C., & Zahn, D.R.T. (2006) Structural And Morphological Properties Of Perylene Derivatives Films On Passivated Semiconductor Substrates. *J. Optoelectron*. Adv. M. 8:604-610.

[11] Beynor, Paez, A., Salvan, G., Scholz, R., Kampen, T.U., & Zahn, D.R.T. (2003) Interaction Of Metals With Perylene Derivatives As A Model System For Contact Formation In OFET Structures. *Proc. Of Spie*. 5217:2010-2017.

[12] Alsalme, A.M., Alghamdi, A.A.B., Al-Baradi, A.M., & Iraqi, A. (2013) Synthesis And Physical Properties Of A "Double-Cable" Polymer For Photovoltaic Applications. *Int. J. Electrochem*. Sci., 8:5575-5593.

[13] Breeze, A.J., Salomon, A., Ginley, D.S., & Gregg, B.A. (2002) Polymer-Perylene Diimide Heterojunction Solar Cells. Appl. *Phys. Lett*. 81. DOI: 10.1063/1.1515362.

[14] Clarke, D., Mathew, S., Matisons, J., Simon, G., & Skelton, B.W. Synthesis And Characterization Of A Range Of POSS Imides. *Dyes Pigments*. 92:659-667.

[15] Erten, S., Meghdadi, F., Gunes, S., Koeppe, R., Sariciftci, N.S., & Icil, S. (22007) Donor-Acceptor Heterojunction Solar Cells Based On Perylene Dimide And Perylene Bisbenzimidazole. *Eur. Phys. J. Appl. Phys*. 36:225-229.

[16] Jin, S.-H., Ban, T., Park, J., Gal, Y.-S., & Lee, J.W. (2013) Synthesis And Photovoltaic Properties Of Low-Band Gap Copolymers Containing Perylene Diimide Derivatives. *Mol. Cryst. Liq. Cryst*. 578:1, 95-103, DOI: 10.1080/15421406.2013.804780.

[17] Kietzke, T. (2007) Recent Advances In Organic Solar Cells. Article ID 40285, 15 Pages. DOI: 10.1155/2007/40285.

[18] Kim, K., Jeong, S., Kim, C., Kim, H., Yang, Y. S., Kim, J. H., Kwon, Y., Tai, W. T. & Han, Y. S. (2010) Synthesis And Optical Properties Of n-Type Polymers

Containing Perylene Moieties, *Molecular Crystals And Liquid Crystals*, 532:1, 29/[445]-38/[454], DOI: 10.1080/15421406.2010.497101.

[19] Kozma, E., & Catellani, M. (2013) Perylene Diimides Based Materials For Organic Solar Cells. *Dyes Pigments*. 98:160-179.

[20] Kozma, E., Kotowski, D., Catellani, M., Luzzati, S., Famulari, A., & Bertini, F. (2013) Synthesis And Characterization Of New Electron Acceptor Perylene Diimide Molecules For Photovoltaic Applications. *Dyes Pigments*. 99:329-338.

[21] Kozma, E., Kotowski, D., Bertini, F., Luzzati, S., & Catellani, M. (2010) Synthesis Of Donor-Acceptor Poly(Perylene Diimide-Altoligothiophene) Copolymers As n-Type Materials For Polymeric Solar Cells. *Polym. J.* 51:2264-2270.

[22] Liang, Z., Cormier, R.A., Nardes, A.M., & Gregg, B.A. (2011) Developing Perylene Diimide Based Acceptor Polymers For Organic Photovoltaics. *Synth. Met.* 161:1014-1021.

[23] Lee, J.W., Choi, Y.S., & Jo, W.H. (2012) Diketopyrrolopyrrole-Based Small Molecules With Simple Structure For High V_{OC} Organic Photovoltaics. *Org. Electron*. 13:3060-3066.

[24] Ozser, M., Yuckan, I., Bodapati, J. B., & Icil, H. (2013) New Naphthalene Polyimide With Unusual Molar Absorption Coefficient And Excited State Properties: Synthesis, Photophysics And Electrochemistry. *J. Lumin*. 143: 542-550.

[25] Pasaogullari, N., Icil, H., & Demuth, M. (2006) Symmetrical And Unsymmetrical Perylene Diimides: Their Synthesis, Photophysical And Electrochemical Properties. *Dyes Pigments*. 69:118-127.

[26] Raj, M. R., Anandan, S., Solomon, R.V., Venuvanalingam, P., Iyer, S.S.K., & Ashokkumar, M. (2012) Synthesis Of Conjugated Perylene Diimide-Based Copolymer With 5,5'-bis(4-Aminophenyl)-2-2'-Bifuryl Moiety As An Active Material For Organic Photovoltaics. *J. Photochem. Photobiol*., A. 247: 52-62.

[27] Rajaram, S., Armstrong, P.B., Kim, B.J., & Fréchet, J.M.J. (2009) Effect Of Addition Of A Diblock Copolymer On Blend Morphology And Performance Of Poly(3-Hexylthiophene):Perylene Diimide Solar Cells. *Chem. Mater*. 21:1775-1779.

[28] Schott, H., Cunow, D.V., & Langhals, H. (1992) Labelling Of Liposomes With Intercalating Perylene Fluorescent Dyes. *Arch. Biochem. Biophys*. 1110:151-157.

[29] Sharma, G.D., Roy, M.S., Mikroyannids, J.A., & Thomas, K.R.J. (2012) Synthesis And Characterization Of A New Perylene Bisimide (PBI) Derivative And Its Application As Electron Acceptor For Bulk Heterojunction Polymer Solar Cells. Org. *Electron*. 13:3118-3129.

[30] Susarova, D.K., Troshin, P.A., Höglinger, D., Koeppe, R., Babenko, S.D., Lyubovskaya, R.N., Razumov, V.F., & Sariciftci, N.S. (2010) Donor-Acceptor Complex Formation In Evaporated Small Molecular Organic Photovoltaic Cells. *Sol. Energy Mater. Sol. Cells.* 94:803-811.

[31] Tahir, M., Sayyad, M.H., Wahab, F., Aziz, F., Shahid, M., & Munawar, M.A. (2013) Perylene Diimide: Synthesis, Fabrication And Temperature Dependent Electrical Characterization Of Heterojunction With p-Silicon. *Physica B.* 426:6-12.

[32] Tan, Z., Zhou, E., Zhan, X., Wang, X., & Li, Y. (2008) Efficient All-Polymer Solar Cells Based On Blend Of tris(Thienylenevinylene)-Substituted Polythiophene And Poly[Perylene Diimide-Alt-bis(Dithienothiophene)].*Appl. Phys. Lett*. 93, 073309(2008); DOI: 10.1063/1.2975160.

[33] Williams, R.M. (2009) A Highly Soluble Asymmetric Perylene-bis(Dicarboximide)-Acceptor System Incorporating A Methylene Bridge Methoxybenzene-Donor: Solvent Dependence Of Charge Transfer IOnteractions. *Turk J Chem*. 33:727-737.

[34] Zhang, X., Wu, Y., Li, J., Li, F., & Li, M. (2008) Synthesis And Characterization Of Perylene Tetracarboxylic Bisester Monoimide Derivatives. *Dyes Pigments*. 76:810-816.

[35] Yang, L., Shi, M., Wang, M., & Chen, H. (2008) Synthesis, Electrochemical, And Spectroscopic Properties Of Soluble Perylene Monoimide Diesters. *Tetrahedron*. 64:5404-5409.

[36] http://pveducation.org/pvcdrom/manufacturing/single-crystalline-silicon

[37] Ali, H.,M. (2014). A Comparison of Photophysical Properties of A Chiral Perylene Monoimide with 3,4,9,10-Perylenetetracarboxylic Acid. Master Thesis, Eastern Mediterranean University.

[38] http://www.rci.rutgers.edu/~dbirnie/solarclass/amorphousSi.pdf

[39] Balzani, V., Credi, A., & Venturi, M. (2003) Molecular Devices and Machines –

A Journey into the Nano World, Wiley-VCH Verlag GmbH & Co. KGaH, Weinheim.

[40] Sun, S. -S., & Sariciftci, N. S. (2005) Organic Photovoltaics Mechanisms, Materials, and Devices, CRC Press, *Taylor & Francis.*

[41] Brabec, C. J. (2003) Organic Photovoltaics: Concepts and Realization, Springer.

[42] Müller, T. J. J. & Bunz, U. H. F. (2007) Functional Organic Materials: Syntheses, Strategies and Applications, Wiley-VCH.

[43] seshadri@mrl.ucsb.edu; http://www.mrl.ucsb.edu/~seshadri/teach.html

[44] http://www.standrews.ac.uk/~www_pa/Scots_Guide/info/comp/passive/diode/pn_junc/pn_junc.htm

[45] http://solarlove.org/solar-cell-model-and-its-characteristics/

[46] http://www.pveducation.org/pvcdrom/solar-cell-operation/iv-curve

[47] February 2010. http://alumni.media.mit.edu/~nate/AES/ PV_Theory_II.pdf

[48] Y. Suita and S. Tadakuma, "Driving Performances of Solar Energy Powered Vehicle with MPTC," IEEE, 2006.

[49] February 2010. http://www.altestore.com/howto/Solar- Power-Residential-Mobile-PV/Off-Grid-Solar-Systems/Electrical-Characteristics-of-Solar-Panels-PV-Modules/a87/

[50] February 2010. http://en.wikipedia.org/wiki/Solar_cell

[51] H. J. Queisser and J. H. Werner, "Principles and Technology of Photovoltaic Energy Conversion," Solid-State and Integrated Circuit Technology, October 1995, pp. 146-150.

[52] T. Maruyama, Y. Shinyashiki and S. Osako, "Energy Conversion Efficiency of Solar Cells Coated with Fluorescent Coloring Agent," Solar Energy Materials & Solar Cells, Elsevier Science, 1998.

[53] S. Capar, "Photovoltaic Power Generation for Polycrystalline Solar Cells and Turning Sunlight into Electricity Thesis," Engineering Physics, University of Gaziantep, July 2005.

[54] X.-J. Ma, J.-Y. Wu, Y.-D. Sun and S.-Q. Liu, "The Research on the Algorithm of Maximum Power Point Tracking in Photovoltaic Array of Solar Car," Vehicle Power and Propulsion Conference, *IEEE,* 2009, pp. 1379-1382.

[55] Hoppe, H., and Serdar, N., S., Linz Institute for Organic Solar Cells (LIOS), Physical Chemistry, Johannes Kepler University, 4040 Linz, Austria.

[56] Bredas, J. –L., Beljonne, D., Coropceanu, V., & Cornil, J. Charge-Transfer and Energy-Transfer Processes in π-Conjugated Oligomers and Polymers: A Molecular Picture. Chem. Rev. 104 (2004): 4971-5003.

[57] Deibel, C., Strobel, T., & Dyakonov, V. Role of the Charge Transfer State in Organic Donor-Acceptor Solar Cells. *Adv. Mater.* 22 (2010): 4097-4111.

[58] Fink, R. F., Seibt, J., Engel, V., Renz, M., Kaupp, M., Lochbrunner, S., Zhao, H.
-M., Pfister, J., Würthner, F., & Engels, B. Exciton Trapping in π-Conjugated

Materials: A Quantum-Chemistry-Based Protocol Applied to Perylene Bisimide

Dye Aggregates. J. *Am. Chem. Soc.* 130 (2008): 12858-12859.

[59] Gratzel, M. Dye Sensitized Solar Cells. *Dye-Sensitized Solar Cells*. J. Photochemistry and Photobiology C: *Photochemistry Reviews. 4* (2003): 145-153.

[60] Lenzmann, F. O., & Kroon, J. M. Recent Advances in Dye-Sensitized Solar Cells. *Advances in Opto Electronics.* (2007): ID 65073.

[61] Brabec, C. J. (2003) Organic Photovoltaics: Concepts and Realization, *Springer*.

[62] Müller, T. J. J. & Bunz, U. H. F. (2007) Functional Organic Materials: Syntheses, Strategies and Applications, Wiley-VCH.

[63] Scaiano, J. C. (1989) (Ed.) Handbook of Organic Photochemistry, CRC press.

[64]Icil, H., & Icil, S. (1997). Synthesis and Properties of a New Photostable Polymer: Perylene-3,4,9,10-tetracarboxylic Acids-Bis-(N,N-dodecylpolymide). *J. Poly. Sci. A: Polym. Chem.* 35, 2137-2142.

[65]Turro, N.J. (1965) Molecular Photochemistry, Benjamin, London, 44.